NANOPARTICLE BASED DRUG DELIVERY TO THE INNER EAR

by

Goncagül Filiz

B.S. Chemistry, Boğaziçi University, 2021

Submitted to the Institute for Graduate Studies in
Science and Engineering in partial fulfillment
of the requirements for the degree of
Master of Science

Graduate Program in Chemistry
Boğaziçi University
2024

Dedicated to my family

ACKNOWLEDGEMENTS

Before anything else, I would like to sincerely thank Prof. Rana Sanyal for her priceless mentoring. Over the course of our three years of working together, she helped me to believe in myself, trusted me, supported me. For that, I am very grateful for her encouragement. She is an excellent woman in science, and I was motivated to follow in her footsteps by her perseverance and achievements. Also, I would like to thank Professor Amitav Sanyal for his counseling and direction on my research. He first introduced organic chemistry while I was an undergraduate, and that's when I knew I had chosen the appropriate field for my career because of his lecture and enthusiasm in chemistry. Thanks to both of my professors' belief in science and their efforts, there are dozens of chemists who have grown up today and dozens of innovations and developments that have been brought to science. They leave the world with priceless legacies because of their determined and disciplined work. I express my gratitude to Asst. Prof. Özgül Gök for accepting to be on my defense jury, as well as for her time, thorough and insightful evaluation of my thesis.

I would like to sincerely thank Damla Demirkol for her friendship, endless support, and guiding me when I did not know what to do, both during my laboratory studies always. I am grateful that she sometimes counseled me and forced me to work more disciplined, her friendship is very valuable to me.

Additionally, I want to thank Ece Günalan İnci for all her assistance in the lab and for giving us the tutorial technical support we required. Although this project was distinct from the Sanyal team's cancer projects, the entire team provided me with companionship and direction whenever I needed it. I express thanks to Dr. Merve Karaçivi, Enfal Çivril, Dr. Aysun Değirmenci and many others in our laboratory team for their friendship, guidance and support throughout my laboratory studies. Thank you for all.

I would like to thank The Scientific and Technological Research Council of Türkiye (TÜBİTAK) for both financial support as part of the 2210-A graduate scholarship program and Euronanomed III transnational funding (TUBITAK project No: 221N356).

Finally, I would like to express my sincere thanks and gratitude to my family for believing in me and for their endless love and support, and to dedicate my thesis to them. Thanks to the power of my mother's love, I am a strong and self-confident woman today. Thank you for always making me feel so lucky, I am glad you exist. Apart from that, endless thanks to Salih Can Egin for his love, patience, understanding, support and taking every step with me, you are my best luck. I have always had strong supporters; I want to sincerely thank Sevil Seyhan and İlayda Fidan for their friendship and support for fourteen years. We dreamt together and knowing that you were with me as we realized them, was my secret strength.

ABSTRACT

NANOPARTICLE BASED DRUG DELIVERY TO THE INNER EAR

As a potential drug delivery vehicle to hair cells in the cochlea of the inner ear, a nanoparticle system was developed. An amphiphilic polymer, a kind of substance with both hydrophilic and hydrophobic characteristics, made up the nanoparticle. The reason polylactide (PLA) was chosen was because it can decompose naturally without harming the environment. Furthermore, PLA is regarded as biodegradable, which makes it a secure choice for a range of biological applications. The initial polymer blocks of polycaprolactone (PCL) and PLA were synthesized using the ring opening polymerization (ROP) process to get the desired diblock copolymer structure. Subsequently, a second polymer block was able to grow after CPADB, a chain transfer agent, was joined to the original blocks. Using reversible addition-fragmentation chain transfer (RAFT) polymerization, the second blocks were grown over the first blocks to produce the diblock polymers PCL-b-p(OEGMEMA) and PLA-b-p(OEGMEMA). Polymeric micelles were prepared using these amphiphilic polymers. It was established their size, drug loading, and stability. The prepared micelles' size, drug loading capacity, and stability were all carefully described. It was discovered that similar micelle sizes, critical micelle concentration (CMC) values, and drug release profiles were caused by the polymers' similar molecular weights and block ratios. The release kinetics of the drug from the micelles was investigated in several buffer solutions, such as Phosphate-buffered saline (PBS), artificial endolymph (a-EL), and artificial perilymph (a-PL), during *in vitro* drug release assays. Notably, with a 5% dexamethasone loading in the a-EL buffer, the release profiles of the PLA-b-p(OEGMEMA) and PCL-b-p(OEGMEMA) were examined and showed similarities.

ÖZET

İÇ KULAĞA NANOPARTİKÜL TEMELLİ İLAÇ İLETİMİ

İç kulağın kokleasındaki tüy hücrelerine potansiyel bir ilaç iletim aracı olarak bir nanopartikül sistemi geliştirilmiştir. Nanopartikülü, hem hidrofilik hem de hidrofobik özelliklere sahip bir tür madde olan amfifilik bir polimer oluşturdu. PLA'nın seçilmesinin nedeni, çevreye zarar vermeden doğal olarak ayrışabilmesiydi. Ayrıca, PLA'nın biyoçözünür kabul edilmektedir, bu da onu bir dizi biyolojik uygulama için güvenli bir seçim haline getirmektedir. PCL ve PLA'nın ilk polimer blokları, istenen diblok kopolimer yapısını elde etmek için zincir açma polimerizasyonu (ROP) kullanılarak sentezlenmiştir. Daha sonra, bir zincir transfer ajanı olan CPADB orijinal bloklara katıldıktan sonra ikinci bir polimer bloğu büyüyebilmiştir. Tersinir ekleme-parçalanma zincir transferi (RAFT) polimerizasyonu kullanılarak, ikinci bloklar PCL-b-p(OEGMEMA) ve PLA-b-p(OEGMEMA) diblok polimerlerini üretmek için ilk blokların üzerinde büyütüldü. Bu amfifilik polimerler kullanılarak polimerik miseller hazırlanmıştır. Boyutları, ilaç yüklemeleri ve stabiliteleri belirlendi. Hazırlanan misellerin boyutları, ilaç yükleme kapasiteleri ve stabiliteleri dikkatlice tanımlanmıştır. Benzer misel boyutları, kritik misel konsantrayon (CMC) değerleri ve ilaç salım profillerinin polimerlerin benzer moleküler ağırlıkları ve blok oranlarından kaynaklandığı keşfedildi. İlacın misellerden salım kinetiği, ilaç salım deneyleri sırasında Fosfat -Salin tamponu (PBS), yapay endeloenf ve yapay perilenf gibi çeşitli tampon çözeltilerinde incelenmiştir. Özellikle, yapay endolenf tamponunda %5 dexamethasone yüklenen PLA-b-p(OEGMEMA) ve PCL-b-p(OEGMEMA) salım profilleri incelenmiş ve benzerlikler göstermiştir.

TABLE OF CONTENTS

LIST OF FIGURES

LIST OF TABLES

LIST OF ACRONYMS/ABBREVIATIONS

ACN	Acetonitrile
a-EL	Artificial Endolymph
AIBN	2,2′-Azobis(2-methylpropionitrile)
a-PL	Artificial Perlymph
BLB	Blood Labyrinth Barrier
BnOH	Benzyl Alcohol
$CDCl_3$	Chloroform
CMC	Critic Micelle Concentration
CPADB	4 -Cyano-4-(phenylcarbonothioylthio) pentanoic acid
CTA	Chain Transfer Agent
DCC	N,N′-Dicyclohexylcarbodiimide
DCM	Dichloromethane
DLS	Dynamic Light Scattering
DMAP	4-(Dimethylamino)pyridine
DMF	Dimethylformamide
EtOAc	Ethyl acetate
EtOH	Ethanol
GPC	Gel Permeation Chromatography
IT	Intratympanic
LC-MS	Liquid Chromotography-Mass Spectrescopy
MeOH	Methanol
Mn	Number average molecular weight
NMR	Nuclear Magnetic Resonance
OEGMEMA	Oligo (ethylene glycol) methyl ether methacrylate
OW(M)	Oval Window (Membrane)
PBS	Phosphate Buffer Saline
PCL	Polycaprolactone
PDI	Polydispersity Index
PLA	Polylactide

RAFT	Reversible Addition- fragmentation Chain Transfer
ROP	Ring Opening Polymerization
RWM	Round Window Membrane
Sn(oct)2	Tin (II) Octanoate
THF	Tetrahydrofuran
UV	Ultraviolet
Vis	Visible

1. INTRODUCTION

1.1. Hearing System and the Cochlea

The process of hearing is a complex and intricate series of events that begins with the entry of sound waves into the outer ear. The pinna, which is the visible part of the ear, acts as a funnel that collects these sound waves and directs them into the ear canal. (Figure 1.1) As the sound waves travel through the ear canal, they eventually reach the tympanic membrane, or eardrum, which responds to the vibrations by vibrating itself. These vibrations are then transmitted to the three small bones in the middle ear: the malleus, incus, and stapes. These bones, known together as the ossicles, act as a megaphone system that amplifies the vibrations and transmits them to the inner ear via the oval window [1].

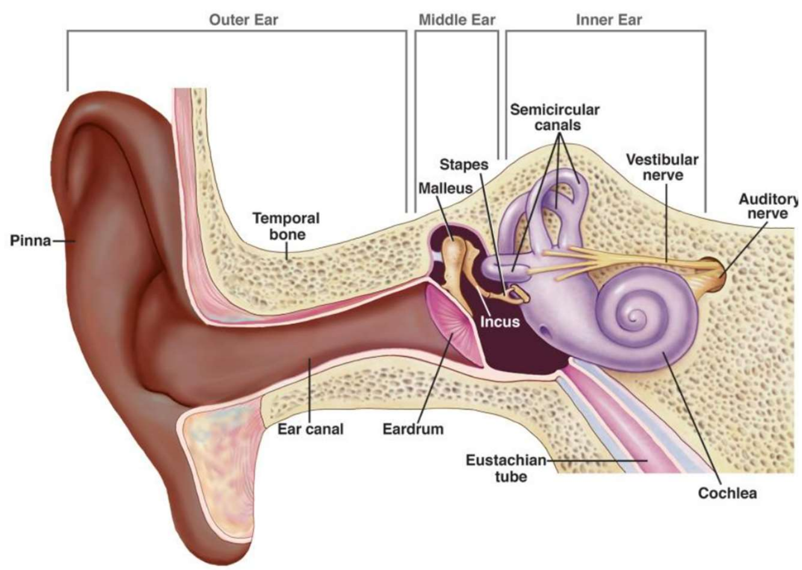

Figure 1.1. The structure of the human ear, partitioned into three parts: outer, middle, inner [2].

In the inner ear, the cochlea, a spiral-shaped structure filled with fluid, plays a crucial role in converting these mechanical vibrations into electrical signals that can be interpreted by the brain. Within the cochlea is an organ called the organ of Corti, which contains specialized hair cells with stereocilia [1]. Delicate hair cells that trigger a nerve impulse when stimulated do the transduction. They are bathed in body fluids, endolymph, that provide energy, nutrients and oxygen because they are alive [3]. When sound vibrations cause the stereocilia to bend, mechanotransduction channels open, allowing potassium ions to enter the hair cells. This influx of ions depolarizes the hair cells and triggers the release of neurotransmitters. These neurotransmitters stimulate auditory nerve fibers, which transmit electrical signals to the brain for processing [4].

It is the brain's interpretation of these signals that ultimately allows us to perceive and understand the sounds we hear, from the soft whisper of a loved one to the roar of a thunderstorm. This complex and coordinated process of hearing attests to human hearing's remarkable complexity and adaptability.

The cochlea, the organ of Corti, and the hair cells need to be examined more closely to fully understand hearing problems. The cochlea contains three fluid-filled chambers - the scala vestibuli, the scala media, and the scala tympani. Reissner's membrane is situated between the vestibular scala and the scala media, and it participates in the regulation of ions. (Figure 1.2.a) Along with the basilar membrane, it creates a cavity within the cochlear duct that is filled with endolymph and located the organ of Corti. The bending of these stereocilia initiates a cascade of events that ultimately leads to the transmission of auditory signals to the brain for interpretation [5]. The stereocilia of the hair cells within the organ of Corti establish connections with the tectorial membrane. (Figure 1.2.b) Alterations in the basilar and tectorial membranes enable the displacement of the stereocilia, subsequently initiating the activation of the hair cell receptors [6].

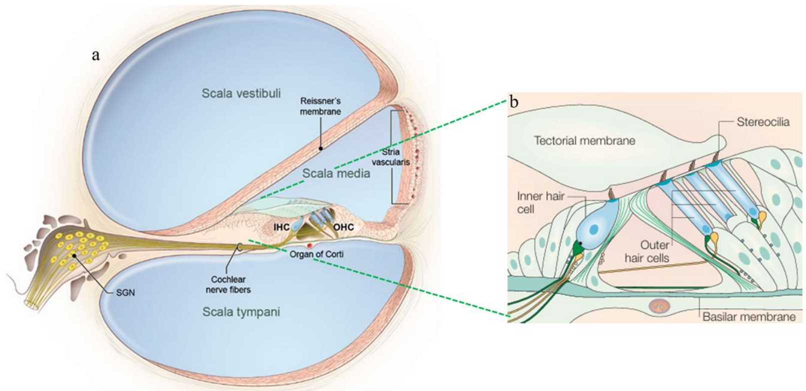

Figure 1.2. The structure of (a) cochlea in cross-section, and (b) sensory part of cochlea, the organ of Corti [7][8].

If the outer hair cells become impaired, their ability to contract in reaction to faint sounds diminishes, consequently leading to a lack of stimulation in the inner hair cells. This results in a reduced capacity to perceive low-intensity sounds. When the sound intensity increases, the inner hair cells are directly activated and exhibit typical responsiveness, thereby preserving the auditory capability to detect louder sounds effectively [10].

1.2. Sudden Sensorineural Hearing Loss and Current Treatment

Hearing impairment stands as the fourth most prevalent form of impairment on a global scale [11]. Over 5% of the global population, equivalent to 430 million individuals, necessitate interventions to address their disabling auditory impairment. Projections indicate that by the year 2050, the number will escalate to over 700 million individuals, representing one-tenth of the populace [12]. The condition under consideration is distinguished by the incapacity to detect sound waves via mechanical oscillations or transmute them into electrical impulses within the neural pathways. Hearing impairment could manifest based on the structure of the auditory system, presenting as either conductive hearing loss resulting from impairment in the external and middle ear, or sensorineural hearing loss (SSHL) arising from injury to the inner ear and auditory nerves [13]. Sensorineural hearing loss is delineated by the deterioration of two categories of cells: cochlear hair cells, which serve as the principal mechanoreceptors for auditory stimuli, and/or auditory nerve neurons, which convey signals from the cochlea to the cochlear nucleus situated in the brainstem, marking the initial stage of auditory processing

[13,14]. SSHL exhibits a multifaceted etiology encompassing both non-genetic and genetic origins. Non-genetic determinants entail exposure to excessive noise, viral infections, persistent inflammation of the middle ear, ototoxic substances like the chemotherapeutic agent cisplatin, aminoglycoside antibiotics, autoimmune disorders, as well as the natural process of aging.

There are various ways to administer drugs to the inner ear, including direct inner ear drug delivery by round window membrane (RWM) and oval window (OW) routes, intratympanic (IT) administration to the middle ear, and systemic administration. (Figure 1.3) Although systemic distribution is among the simplest to administer, it is impeded by the blood-labyrinth barrier (BLB), which keeps blood circulation and inner ear fluids apart [16,17]. Despite the fact that the drug molecules can enter the inner ear through systemic administration, the local drug concentration is frequently below the therapeutic threshold due to the restricted local blood supply and inadequate BLB penetration [18]. Large doses of medications are required to get the desired therapeutic effect, which frequently results in severe ototoxicity. Additionally, as it directly avoids numerous biological barriers, direct inner ear drug delivery via RWM and OW pathways may be more effective, while it has significant drawbacks. Injecting into these windows requires surgery, which carries a risk of trauma and the potential for postoperative complications [19]. As opposed to systemic administration, which avoids the side effects of high-dose medication, IT injects the drug into the middle ear space, allowing it to diffuse to the inner ear through the RWM, avoiding the BLB [20]. Compared to oral or non-injection, the drug concentration of IT injection was considerably higher in the inner ear fluid, perilymph, and endolymph [20, 21].

The concentration of drug reaching the inner ear depends on the dose of drug contacting the RWM circular window membrane of the middle ear, and variations in RWM permeability will alter drug retention and elimination rates [20, 22]. Despite the high efficiency of IT administration and its ability to lessen the toxic and side effects of systemic administration, formulating a standard dosing regimen becomes challenging.

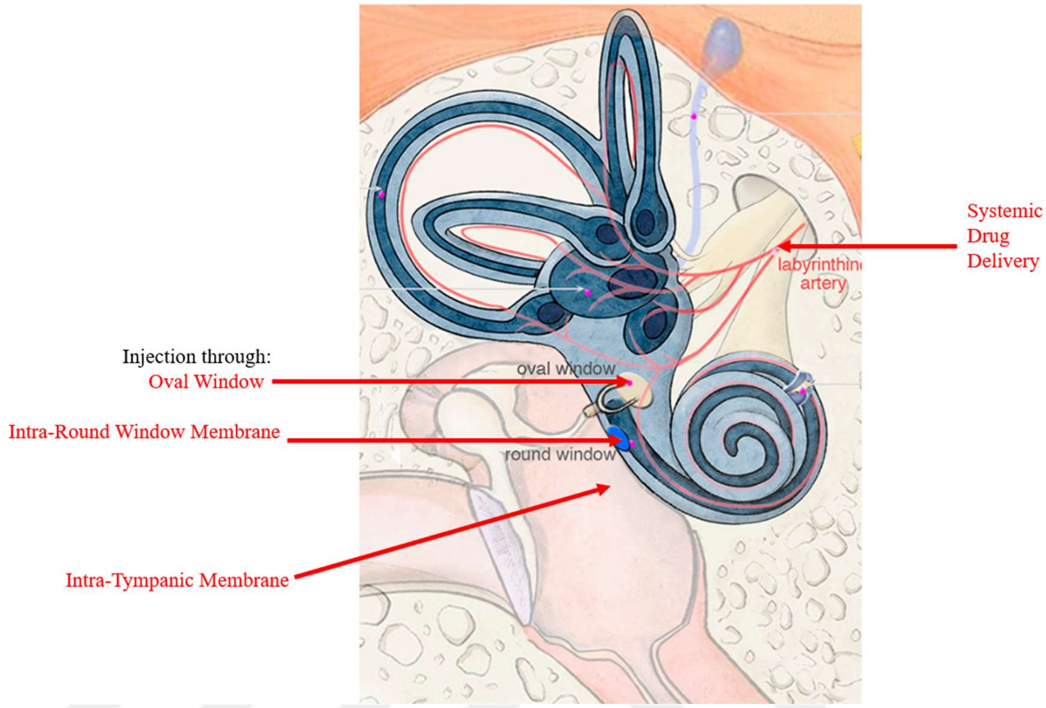

Figure 1.3. Possible anatomical routes for therapeutic delivery into the inner ear [15].

Three layers comprise the RWM; an epithelial layer that faces the middle ear, a layer of connective tissue that lies between, and an epithelial layer that faces the cochlea's scala tympani [23]. Because the RWM is semi-permeable, drugs with low molecular weight, high lipid solubility, and positive charge typically diffuse more readily [24]. Since many anionic proteins are present on cell surfaces, cationic substances can flow across the RWM more readily [25]. The stapes footplate closes the oval window, which divides the middle ear from the scala vestibuli (Figure 1.3). For this reason, drug delivery via the oval window has not received as much research attention as drug administration via the RWM.

1.3. Nanocarriers to the Inner Ear

Nanocarriers have changed the landscape of drug delivery methodologies and represent a promising solution to overcome various obstacles in targeting specific tissues or organs. In the field of drug delivery to the inner ear, the use of nanocarriers by intratympanic route has emerged as a particularly innovative strategy. Using nanocarriers, drugs can be encapsulated and delivered directly to the inner ear, by passing the blood- labyrinth barrier, and reducing systemic side effects. This precise delivery technique has significant potential in the treatment of inner ear disorders such as hearing loss or tinnitus, providing a more effective and streamlined approach to delivering therapeutic agents to the site of action [27].

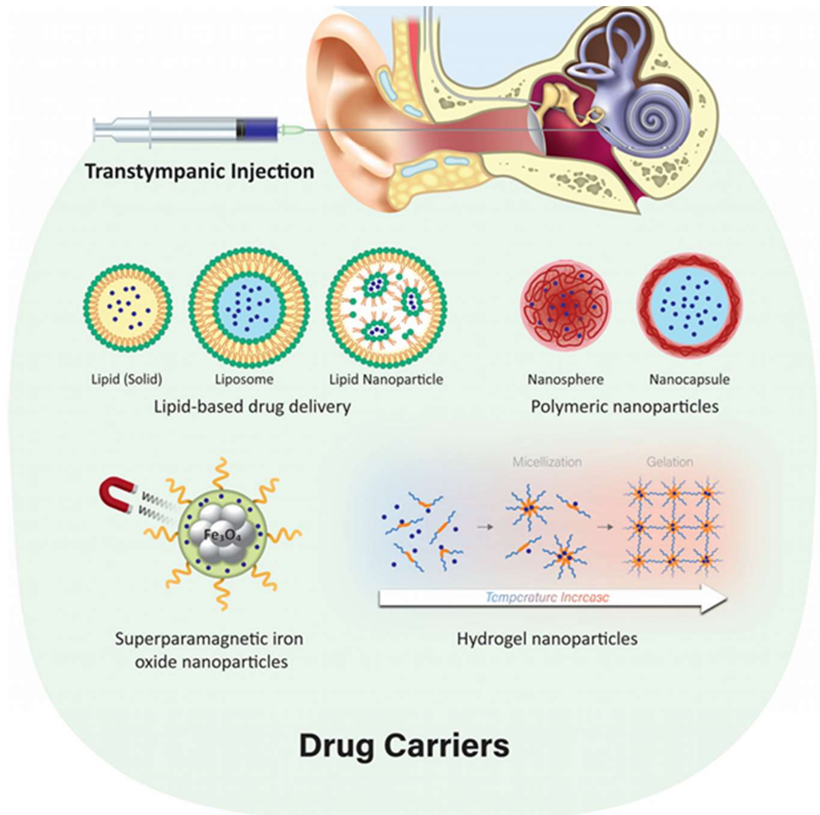

Figure 1.4. Intratympanic injection of biomaterials to the RWM for inner ear therapy [26].

The development of biomaterials that overcome cellular toxicity, regulate degradation kinetics, and modulate drug dispersion after delivery requires attention. Two primary categories of biomaterials have been developed to prolong delivery, limit degradation, and provide uniform distribution within the inner ear: hydrogels and nanoparticles [28] (Figure 1.4). Soluble drugs can be incorporated into hydrogels positioned at the RWM for controlled and sustained drug diffusion from the middle ear compartment. The attachment of drugs to nanoparticles impedes drug degradation and can be fine-tuned for rapid diffusion and specific targeting of cells within the inner ear [29]. The formulation of such biomaterials requires taking persistent breakdown, toxicity, and efficacy into account. To work safely and successfully as a therapeutic delivery system, the specifications for each targeted organ must be specifically designed and customized. In order to do this, biomaterial methods for inner ear medication delivery have been developed quickly thanks to recent developments in material science and nanochemistry.

Nanoparticles can be tailored to encapsulate different therapeutic substances and are made from a range of materials with diameters ranging from 10 to several hundred nanometers [30]. Drug stabilization controlled or sustained release, non-invasive administration, and surface modification to target certain organs are all common uses for nanoparticles [31]. Biomaterials have been successfully delivered into the inner ear in several experiments that used nanoparticles applied to the RWM [32]. Nanoparticles can be directed to a particular intracochlear region of interest and can penetrate both the perilymph and the endolymph [33] after intratympanic injection. When hydrogel and nanoparticles are mixed, the medication's bioavailability at the intended site is increased and fast drug release is avoided [33]. Additionally, nanoparticles can have their surfaces altered to improve their engagement with RWM, or they can be coupled to peptides that could enter cells [34]. Poor drug uptake by inner ear cells and restricted access to the inner ear are obstacles to nanoparticle administration into the inner ear [33]. Liposomes have several drawbacks, such as limited encapsulation effectiveness for lipophilic pharmaceuticals and the potential for the marketed product to be unstable and leaky in biological or aqueous fluids if their composition calls for organic solvents [35]. The use of SPIONs in humans is restricted due to their decreased biodegradability and adverse consequences, which include genotoxicity, inflammation, reactive oxygen species production, and a longer duration of residency in the cochlea [36,37].

1.3.1. Pharmacokinetics of Nanocarriers Drugs to the Inner Ear

The term "pharmacokinetics" refers to how medications flow through the body. Adsorption, distribution, metabolism, and excretion are all included. Due to the interaction of numerous factors, including drug passage through the RWM, distribution in perilymph and endolymph, different ear tissue compartments, and clearance into cerebrospinal fluid via the cochlear aqueduct, the pharmacokinetics of locally applied drugs within the inner ear are complex [38]. Drugs are absorbed when they diffuse into the perilymph from the middle ear through the cochlear bone shell, the RWM, or the OWM [39]. Following systemic administration, absorption involves the medication being trafficked over the blood–labyrinth barrier from the vascular system into the inner ear [40]. The intracochlear dispersion of medications in the perilymph, endolymph, and inner ear tissues is described in distribution. It is dependent upon multiple parameters, including blood flow, lipid solubility, and drug permeability. Additionally, distribution is gradient-dependent on concentration [38]. The chemical process by which medications are changed into more bioactive metabolites, especially in the liver, is referred to as metabolism [40]. Once absorbed into the inner ear, the prodrug dexamethasone phosphate—which is frequently administered transtympanically—converts into an active form [41]. The process of removing a medication or its metabolites from the body is known as elimination [38]. Drugs or their metabolites can be removed from cochlear fluid into cochlear cells, blood, CSF, and the middle ear in the inner ear [38]. It can be removed from the middle ear by passing through the Eustachian tube and into the nasopharynx [40]. The excretion through the Eustachian tube is slower the higher the drug's viscosity. Drug metabolism or structural degradation can also result in a decrease in drug concentrations [38].

1.4. Polymeric Micelles as Nanocarriers

Biodegradable polymeric microparticles, sometimes known as nanoparticles, have been developed for a variety of medicinal uses, including the administration of medications intended for the inner ear. They have several advantages over other delivery methods because of their tiny size, high degree of consistency in formulation, biocompatibility, and biodegradability [42]. The majority of nanoparticles have a diameter of less than one micrometer; formulations often have a diameter of 100 to 300 nm, and for inner ear delivery, the diameter should be 200 nm or less [43]. In the case of amphiphilic polymeric particle that can encapsulate hydrophilic and hydrophobic drugs for intratympanic delivery, allowing transcellular passage through the round window membrane (RWM) and into the perilymph [44].

Most polymeric micelles are self-assembled nanoparticles that are produced at concentrations above the critical micelle concentration (CMC) from amphiphilic or multifunctional block copolymers. The structure of these polymers may attract and repel water in aquatic conditions, leading to the creation of the hydrophilic corona and hydrophobic core of polymeric micelles. These polymers have end-to-end hydrophobic and hydrophilic chains. Hydrophobic interactions allow hydrophobic drug moieties to be successfully encapsulated in the core of polymeric micelles [45]. Depending on the block polymer's structure, there are various ways that block copolymers can self-assemble (Figure 1.5).

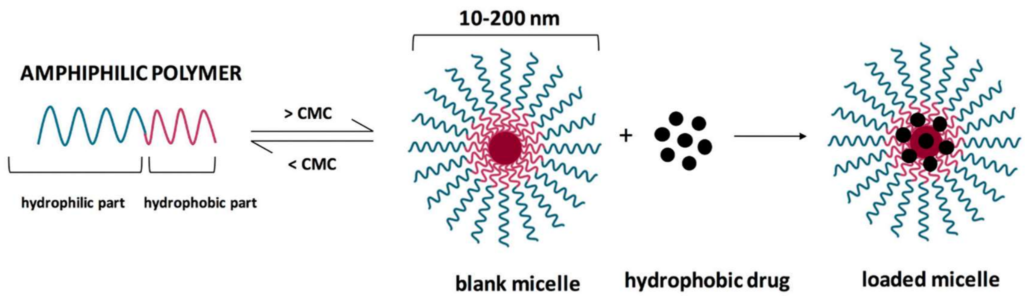

Figure 1.5. Schematic representation of polymeric micelles [46].

When the drug and polymer are insoluble in water, cosolvent evaporation is employed to create polymeric micelles. Using this process, water is introduced dropwise to create emulsions after the polymer and drug are combined in water miscible volatile solvents. Polymeric micelles suspended in water are present in the solution after volatile solvents evaporate [47]. The degree of contact between drug molecules and the micellar core is essential for polymeric micelle drug release kinetics, drug loading, encapsulation efficiency, and micellar stability [47]. The primary deterministic elements in these features are typically hydrogen-bonding and hydrophobic interactions [48]. The molecular weights, chemical structures, and CMC values of the polymers that are utilized as building blocks affect the properties of polymeric micelles as well. It is possible to modify the amphiphilic block copolymers to give the micellar nanoparticle the necessary characteristics.

1.4.1. Drug Release from Polymeric Micelle

Drug release from intact micelles or micelle disintegration can result in drug release from polymeric micelles (Figure 1.6). In any case, micelles need to have strong thermodynamic and kinetic stability to prevent an uncontrolled drug release during administration [49, 50]. Consequently, several physicochemical techniques have been put out and discussed in a recent study to prevent the system from disintegrating too quickly or to stabilize the medication that has been encapsulated in the micellar core.

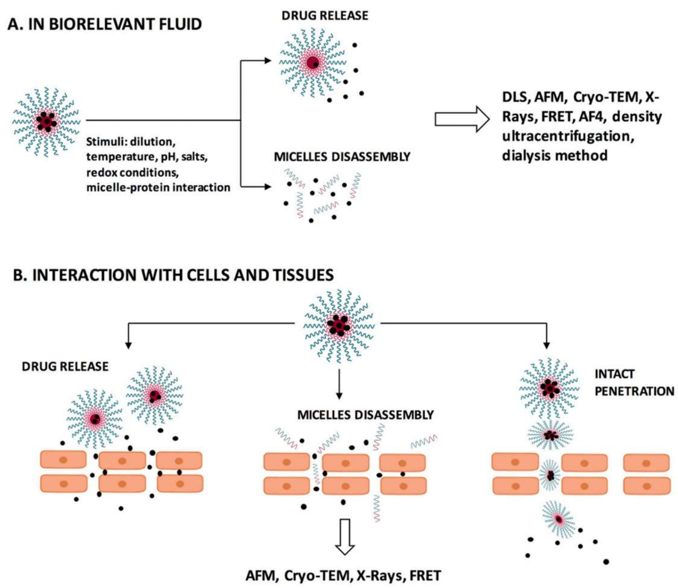

Figure 1.6. Schematic representation of drug release and micelle interaction with the biological fluids (A) and with cells and tissues (B) the techniques that could be used to study drug release [46].

For example, block copolymers conjugated with a lipid molecule were synthesized because it is well-known that a decrease in the CMC can be obtained by increasing the length of the hydrophobic section of the block polymer [49, 51]. Additional tactics include the crosslinking of the micelle's core, the functionalization of the hydrophobic block [52], or the creation of a conjugate between the drug and the polymer such that the drug is only released once the bond breaks. Since proteins from plasma or intracellular fluids can be absorbed on the surface of micelles, forming the so-called protein corona, which partially obscures the outer shell functional groups and modifies the physiological response of nanocarriers in terms of biodistribution, cellular uptake, metabolism, and toxicity, it is important to investigate the structural stability of micellar systems under biorelevant conditions [53, 54-56]. Serum proteins have been shown to be crucial for the stability of micelles by encouraging their rupture or aggregation [57, 58]. After topical administration to cutaneous and mucosal tissues, micelles have been reported to contain additional sources of instability [59, 60]. In fact, the interaction of micelles with mucus, epithelia, stratum corneum lipids, and sebum can be observed to cause their disaggregation, while the interaction of the micelles with the lacrimal fluid may lead to drug precipitation due to competition with solutes found in the tear film. Finally, it is important to highlight the vigorous current research on stimuli-responsive polymeric micelles, which could adjust drug release in response to a variety of impulses, both artificial and biological (such as ultrasounds, magnetic fields, or temperature changes) and biological (such as acidic pH, redox potential, or particular enzymes) [61].

1.5. Polymerization of Nanocarriers

The development of polymer chemistry has opened a wide range of possibilities for designing polymers with unique architectures, high homogeneity, regulated molecular weights, and the conjugation of various monomers and reactive groups to the polymer backbone. Ring-opening polymerization (ROP), reversible addition-fragmentation chain-transfer polymerization (RAFT), and atom transfer radical polymerization (ATRP) are a few controlled chain growth dependent polymerization techniques. Ring-opening polymerization (ROP) and Reversible Addition-Fragmentation Chain Transfer (RAFT) polymerization are the polymerization techniques used in this thesis.

1.5.1. Ring Opening Polymerization

ROP process is one of the three major pathways to creating polymers, alongside chain (radical and ionic) polymerization and condensation polymerization [62]. ROP is particularly valuable for synthesizing polymers with specific properties and applications.

The process begins with the initiation phase, which is the activation of a cyclic monomer. A variety of initiators, which cleave a link within the monomer, help to open the ring. Examples of these include metal alkoxides and organic molecules. The propagation phase then starts, in which the activated monomer interacts with a different monomer unit to form a growing polymer chain. As the ring opens, the monomer integrates into the polymer chain. The polymerization process persists as additional monomers join the chain. The final stage is termination; however, ROP excludes termination steps like radical or ionic termination [63]. The process endures until all monomers are expended or until specific conditions, such as temperature or concentration, interrupt the reaction.

Ring strain in the cyclic monomer frequently acts as the catalyst for ROP. The reaction route is mostly determined by steric hindrance and spatial constraints. The process's overall thermodynamics are influenced by the strain energy released upon the ring opening [64].

1.5.2. Reversible Addition-Fragmentation Chain-Transfer Polymerization

A certain method for live-controlled radical polymerization is called RAFT polymerization. It creates polymers with the appropriate molecular weights and low polydispersity index values using a chain transfer agent (CTA) and radical initiator. The polymerization of (meth)acrylates, (meth)acrylamides, styrene and their derivatives, vinyl groups conjugated to a double bond, and nitriles such as acrylonitrile are the main applications for it [65, 66]. Depending on how the RAFT agent (CTA) is constructed, polymers with a range of end groups, such as those that permit the coupling of bioactive compounds, can be created via RAFT polymerization [67].

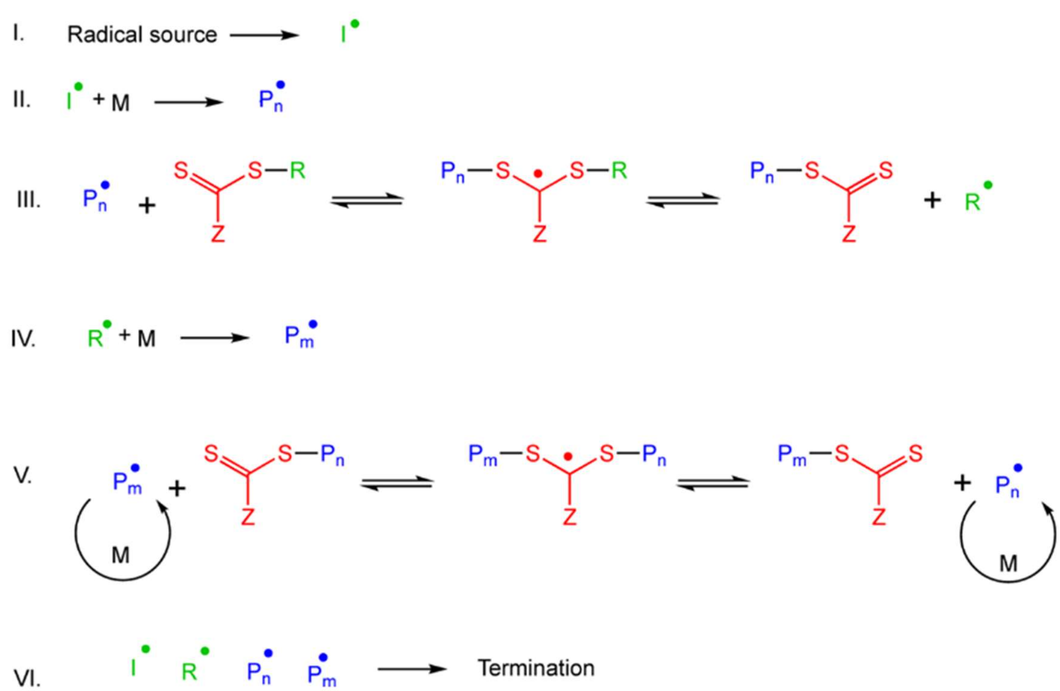

Figure 1.7. Mechanism of RAFT Polymerization [65].

The main point of the RAFT polymerization mechanism (Figure 1.7) is a degenerative transfer-achieved equilibrium between dormant and active chains. The total amount of radicals in this system remains constant during the activation-deactivation process. The activation step is the first stage, during which the radical species were discovered. [68] Next, the monomer is attacked by the acquired radical, and polymerization begins. In stages III and V, the obtained macromolecules containing the radicals were introduced to the RAFT agent (chain transfer agent, CTA) to achieve equilibrium between active and dormant species. The chain transfers phases that make up the foundation of the RAFT process create its base. Between the inactive chains of CTA, which are normally the Z−C(=S)S, functional R group, and thiocarbonylthio group, chains were degenerated. Effective polymerization will result in a rate of addition/fragmentation equilibrium that is higher than the rate of propagation. Stated differently, it is recommended to add less than one monomer unit every activation cycle, as this will lead to a very close degree of polymerization (DP) and a low polydispersity index (PDI) [65, 66]. For a variety of reasons, RAFT polymerization is a widely used method in the production and design of polymer drug conjugates [69]. It makes it possible to create block polymers and functional copolymers. Chain ends of polymers can be post-modified, and a variety of organic chemical techniques are available for this functionalization.

2. AIM OF THE STUDY

The primary objective of this study was the development of drug loaded polymeric micellar nanoparticles from two amphiphilic block copolymers to be used for localized treatment of hair cells in the inner ear. The inner ear, where the hair cells are located, is a challenging target for systemic drug therapy due to the limited accessibility and the sparse, small blood vessels in this region. Polymeric micellar nanoparticles, which can improve drug stability, provide controlled release, and facilitate transport through the endolymph to the target side, have emerged as a promising drug delivery system. Currently, local drug therapy for the inner ear is very limited. In addition, the cost and daily life challenges associated with in-the-ear and behind-the-ear hearing aids are significant. Therefore, the objective of this study was to investigate the successful synthesis of dexamethasone loaded amphiphilic block copolymers PLA-b-p(OEGMEMA) and PCL-b-p(OEGMEMA), and their self-assembly into stable, drug-loaded polymeric micelle nanoparticles. In addition, the study sought to evaluate the *in vitro* drug release profiles from these micelles, which could potentially lead to improved treatment options for inner ear disorders.

3. EXPERIMENTAL

3.1. Materials

All reagents were obtained from commercial sources and were used as received unless otherwise stated. Dry solvents such as dichloromethane (DCM), tetrahydrofuran (THF) and toluene were obtained from ScimatCo Purification System, other dry solvents were dried over molecular sieves. All solvents including N, N-Dimethylformamide (DMF), acetonitrile (ACN), ethyl acetate (EtOAc), N, N-Dimethylacetamide (DMAC), methanol (MeOH), dichloromethane (DCM), diethyl ether and deuterated chloroform ($CDCl_3$) were HPLC grade, purchased from Merck and used without further purification. Lactide, □-caprolactone, 4-Cyano-4-(phenylcarbonothioylthio) pentanoic acid (CPADB), $Sn(Oct)_2$, N,N'-Dicyclohexylcarbodiimide (DCC), benzyl alcohol (BnOH), pyrene, 2,2' azobisisobutyronitrile (AIBN) were purchased from Sigma Aldrich. Poly (ethylene glycol) methyl ether methacrylate (Mn = 300) (OEGMEMA, 99%) was also purchased from Sigma Aldrich and was filtered with basic alumina column to remove inhibitor. Dexamethasone was purchased from DEVA Holding Inc. The dialysis bags (Spectra/Por® Biotech Regenerated Cellulose Dialysis Membranes, MWCO 3.5 kDa) were purchased from Spectrum Labs.

3.2. Instrumentation

^{1}H NMR spectroscopy (Bruker 400 MHz spectrometer) was used to characterize functionalized polymers at 25°C. Deuterated chloroform ($CDCl_3$) was used as the NMR solvent. Gel permeation chromatography with a Shimadzu PSS-SDV column (length/ID 8 x 300 mm, 10 µm particle size), 0.05 M lithium bromide in DMAC as the eluent and a flow rate of 1.0 mL/min was used to analyze the molecular weights and polydispersity index (PDI) values of the synthesized polymers. Varian Cary 100 UV-Vis Scan spectrophotometer was used to obtain UV-vis. spectra. At room temperature, the Varian Cary Eclipse Spectrophotometer was used to measure the fluorescence spectrum. The rectangular quartz cuvette has a 1 cm route length. Malvern Zetasizer Nano ZS photometer was used to obtain dynamic light scattering (DLS) results, also fluorescence spectroscopy using a Cary Eclipse Fluorescence

Spectrophotometer. Concentrations of dexamethasone in solutions in drug release or drug loading studies were also measured using LC-MS (Shimadzu, Japan).

3.3. Synthesis of PLA

The synthesis of the polylactide block, which forms the hydrophobic block, was the first part of the diblock polymer synthesis.

Lactide must be crystallized to purify it before it can be polymerized. Lactide crystals were distilled three times in EtOAc and EtOH at 70 °C for 1 h (10 g lactide was crystallized with 10 mL EtOAc and 20 mL EtOH) to completely remove moisture. After each distillation, it was allowed to recrystallize at +4 °C for 5 h. After the third distillation, lactide was washed with toluene and dried at 45 °C in a rotary evaporator, followed by drying under high vacuum for 12 h.

For the first block polymerization, lactide (1 g, 6.94 mol), BnOH (10.72 mg, 0,09921mmol) and $Sn(Oct)_2$ (10 mg, 0.0248 mmol) (stock solution was prepared with toluene) were placed in a round bottom flask at room temperature and ring opening polymerization took place for 1 h after the crystal lactide melted at 100 °C under high vacuum. After the lactide melted, the magnetic stirrer stopped rotating and the mixture changed from white to colorless. At the end of the reaction time, the flask was disconnected, vacuum was disconnected, and the reaction was left at 120 °C for 22 h. Contact with air was made to stop the reaction, the formed polymer was still colorless. Obtained PLA was dissolved with a minimum amount of acetone (about 4 mL) and precipitated dropwise in a mixture solution of diethyl ether and EtOH (2:1, v/v), the colorless solution turned turbid white when PLA was added. The solution was kept at -20 °C overnight for precipitation, the precipitated polymer was then dissolved with acetone both from the bottom of the Erlenmeyer flask and from the wall of the flasks after centrifugation. The precipitation was repeated two more times in diethyl ether only. After evaporation of acetone in a rotary evaporator at 35 °C, the obtained PLA was left overnight in high vacuum (612 mg, 60 % yield). ^{1}H NMR (CDCl3, δ, ppm): 7.3-7.4 (m, 5H), 5.34 (m, 2H), 5.17 (s,1H)

3.4. Synthesis of PCL

e-Caprolactone (1 g, 8.76 mmol) and BnOH (10.9 mg, 0.10 mmol) were placed in a 10 mL round bottom flask. $Sn(Oct)_2$ (5.5 mg, 0.01 mmol) was dissolved in anhydrous toluene and added to the round bottom flask. The vacuum flow control adapter was placed on top of the round bottom flask and the junction was wrapped with Teflon tape to prevent moisture ingress. The solution was kept under high vacuum at 90 °C for 1 hour to remove water. After 1 hour, it was removed from vacuum and stirred at 120 °C for 22 h with the help of a magnetic stirrer. When the reaction was completed, the solidified product was dissolved in 3 mL THF and precipitated in 200 mL cold diethyl ether to get rid of unreacted monomers. Solution was kept at -20 °C overnight to increase the amount of precipitated polymer, then the precipitated polymer was collected by centrifugation and dried under high vacuum in a vial (712 mg, 77 % yield). ^{1}H NMR (CDCl3, δ, ppm): 7.35 (m, 5H), 5.11 (s, 2H), 4.05 (t, 244H of repeating unit), 3.65 (t, 2H)

3.5. Synthesis of Macroinitiators PLA-CTA and PCL-CTA

For the synthesis of the macroinitiator PLA-CTA, PLA, CPADB (7.9 mg, 0.0284 mmol), DMAP from stock solution and the solvent DCM were purged in a round bottom flask with N_2 gas for 15 min to remove O_2. DCC from stock solution was added to the flask under ice bath, and solution was purged for another 15 min. The DCC/DMAP coupling reaction (pink transparent color) occurred in the dark at room temperature for 24 h. The flask was covered with aluminum foil to protect the CPADB from light. The reaction was stopped by contact with air and the solvent was evaporated in a rotary evaporator at 30-35 °C. The product remaining at the bottom of the flask was dissolved with THF. The by-product DCU (dicyclohexylurea) that is white solid, was precipitated and removed by centrifugation. The formed pink translucent PLA-CTA was precipitated three times in MEOH and was kept at -20 °C overnight to increase the amount of precipitated polymer. After precipitation, PLA-CTA was dissolved with THF, taken in a vial and THF was evaporated in a rotary evaporator. PLA-CTA was kept overnight in high vacuum (79 mg, 80 % yield). ^{1}H NMR (CDCl3, δ, ppm): 7.9 (2H), 7.6 (1H), 7.3-7.4 (7H), 7.22 (2H), 5.17 (1H), 4.3 (3H), 2.75 (2H)1.7-1.8 (5H) 1.56 (3H).

The same procedure was followed for the synthesis of macroinitiator PCL-CTA using the synthesized PCL (100 mg, 0.0071 mmol), CPADB (7.78 mg, 0.0279 mmol), DMAP (0.682 mg, 0.00559 mmol), and DCM (0.5 mL). PLA-CTA was obtained after purification by precipitation (98.44 mg, 92 % yield). ^{1}H NMR (CDCl3, δ, ppm): 7.90 (3H), 7.57 (1H), 7.35 (7H), 4.05 (244H of repeating unit), 2.65 (4H)

3.6. Synthesis of Diblock Polymers PLA-b-p(OEGMEMA) and PCL-b-p(OEGMEMA)

The second block of both diblock polymers consisted of OEGMEMA (Mw 300 g/mol), which was filtered with Al_2O_3 to get rid of BHT (2,6-bis(1,1-dimethylethyl)-4-methylphenol) before the reaction. BHT plays the role of free radical trapping and prevents the self-polymerization of OEGMEMA during storage. AIBN was stored in toluene solution and was dried in a rotary evaporator at 25-30 °C until the solvent evaporates and then left overnight in high vacuum before using for polymerization.

For the synthesis of PLA-b-p(OEGMEMA), OEGMEMA (154.72 mg, 0.515 mmol), PLA-CTA (100 mg, 0.00573 mmol) as macro initiator and DMF (0.4 mL) were purged in a round bottom flask with N_2 gas for 15 min. AIBN (0.18 mg, 0.0011 mmol) from prepared stock solution in DMF was added and solution was purged with N_2 gas for a further 15 min. Reversible addition-fragmentation chain transfer (RAFT) polymerization occurred for 23 h at 70 °C. The reaction was stopped by contact with air and DMF was evaporated at 45 °C using rotary evaporator. The solid product PLA-b-p(OEGMEMA) (polylactide-b-poly (oligo (ethylene glycol methyl ether methacrylate)) was dissolved with DCM and precipitated in cold diethylether at -20 °C overnight. The solution and orange pink diblock product were separated by centrifugation. The precipitated product PLA-b-p(OEGMEMA) was dissolved with DCM and dried on a rotary evaporator and then under high vacuum. (84.24 mg, 72 % yield). ^{1}H NMR (CDCl3, δ, ppm): 7.9 (2H), 7.6 (1H), 7.3-7.4 (7H), 7.22 (2H), 5.17 (1H), 4.3 (3H), 3.6-3.7 (4H)

For the synthesis of PCL-b-p(OEGMEMA), PCL-CTA was used as the macroinitiator (100 mg, 0.00833 mmol), using OEGMEMA (250 mg, 0.833 mmol), AIBN (0.68 mg, 0.00416 mmol), and DMF (1.25 mL) and following the same procedure as PLA-b-p(OEGMEMA) synthesis. (245 mg, 70 % yield). ^{1}H NMR (CDCl3, δ, ppm): 4.05 (244 H of repeating unit), 3.38 (123 H of repeating unit).

3.7. Critical Micelle Concentration (CMC) Measurements

The synthesized diblock polymers PLA-b-p(OEGMEMA) and PCL-b-p(OEGMEMA) were separately dissolved with THF, and stock solutions were prepared. For each polymer, specified volumes from these stock solutions were taken in separate vials to obtain final polymer concentrations ranging from 4 x 10^{-5} M to 4 x 10^{-9} M in 3 mL water. A pyrene stock solution was prepared and 10 mL of this stock solution was put in each vial so that 6 x 10^{-7} M pyrene was present in each sample in 3 mL water. In vial 1, no polymer was added, the dye was used as a control sample. At the end total THF volume was 700 µL in all samples. After adding the organic solvent, 3 mL of distilled water was added dropwise to each sample. The organic solvent THF was evaporated in a well-ventilated hood overnight at room temperature. The experimental procedure was used to determine the CMC value of diblock polymer sample, and all are read on a fluorescence spectroscopy device. Excitation spectra of fluorescent probe Pyrene was recorded between 300 nm and 360 nm, with the emission wavelength set at 390 nm. The CMC values were calculated by analyzing the ratio between the fluorescence intensities at 338 nm and 334 nm as a function of the logarithm of the polymer concentration.

3.8. Formation of Polymeric Micelles

Diblock polymer PLA-b-p(OEGMEMA) or PCL-b-p(OEGMEMA) (3 mg) and dexamethasone were used to obtain dexamethasone loaded polymeric micelles. For 5 % dexamethasone loaded micelles, 0.158 mg dexamethasone was used. Similarly, for 10 %, 0.334 mg, for 15 %, 0.530 mg, and for 20 % 0.750 mg of dexamethasone was used while keeping the amount of diblock polymer constant. Polymer stock solution was prepared to contain desired polymer in 700 mL and drug stock solution in 300 mL THF, and after combining these stock solutions in a 10 mL round bottom flask, 2 mL of distilled water was added dropwise to the mixture. THF was evaporated in a rotary evaporator at 37 °C, 80 rpm, 100 mbar for 12 min to form drug-loaded micelles in the water. The obtained micelle solution was centrifuged at 13000 rpm for 5 min and the drug that did not enter the micelle was precipitated, then solution was filtered through a PTFE 0. 45µm filter.

The size and PDI of the micellar nanoparticle were determined by DLS measurements. For the quantification of the drug loaded into the micelle, the sample was diluted tenfold with ACN to burst the micelles and release the drug inside them and submitted to LC-MS. A calibration curve for dexamethasone between 5 mg/L and 100 mg/L was used to determine drug loading.

3.9. Stability of Polymeric Micelles

To measure the stability of dexamethasone-loaded micelles, 1 mL nanoparticle samples containing 1 x 10^{-5} M diblock polymer concentrations were subjected to serial dilution with water. To determine the stability of the nanoparticles against dilution with water, the volume was diluted twofold each time. The solution was then diluted twofold by pipetting 500 µL and mixing with 500 µL distilled water.

The percentage by volume of nanoparticles in the solution and the average sizes of the diluted PLA-b-p(OEGMEMA) and PCL-b-p(OEGMEMA) micelles in the total particles were measured by DLS. The dilution and DLS measurement process was repeated up to a dilution factor of 2048 for PLA-b-p(OEGMEMA).

3.10. *In vitro* Drug Release from Polymeric Micelles

Stability and release tests setup were to analyze the stability of dexamethasone in PBS (Phosphate-buffered saline) and artificial fluids inside the ear such as artificial endolymph (a-EL) and artificial perilymph (a-PL) and the behavior of dexamethasone molecules exiting the hydrophobic interior of the polymer and mixing into the buffer liquid.

The PBS used in the tests was prepared first as 100 mM $Na_2HPO_4.2H_2O$, 17.63 mM KH_2PO_4, 1.3689 M NaCl and 0.6 mM KCl at ten-fold concentration (PBS 10x). After ten-fold dilution, the pH value was adjusted to 7.4 with 12 M HCl (PBS 1x). Artificial endolymph fluid was prepared according to literature [70], which contained 31 mM $KHCO_3$, 126 mM KCl, 1.3 mM NaCl, 0.023 mM $CaCl_2$ and 0.6 mM glucose, then pH was adjusted to 7.4 with 12 M HCl. 10 mL of the buffer solutions were taken in a vial and brought to body temperature (37 °C) before starting release experiments.

Dexamethasone-loaded micelles were prepared with PLA-b-p(OEGMEMA) and PCL-b-p(OEGMEMA) according to 10/5/1 wt% drug loading (DL). Micelle solutions containing PLA-b-p(OEGMEMA) (4.75 mg, 0.000139 mmol) and dexamethasone (0.25 mg, 0.000637mmol) in each 1 mL of solution were prepared by cosolvent evaporation as described above to perform the *in vitro* drug release studies. 1 mL of the micellar solution was taken in a dialysis bag made from a dialysis membrane with a 3.5 kDa molecular weight cut-off, and the bag was immersed in 10 mL buffered solutions (pH 7.4). At the time of sampling, 100 μL of buffer was removed and 100 μL of fresh buffer was added to the release vial. Using a calibration curve for dexamethasone between 5 mg/L and 100 mg/L, drug concentrations in the samples were analyzed by LC-MS.

For dexamethasone stability tests, 40 ppm dexamethasone solution was obtained by diluting the 1000 ppm dexamethasone stock prepared with ACN with PBS or other buffers. Samples were taken without adding fresh buffer. Stability and release samples were taken from the test tube every 15 minutes for the first hour and every hour for the first 8 hours and analyzed in LC-MS. While dexamethasone could remain intact in PBS for the first 48 hours, it was found that it started to degrade in artificial endolymph at the 8th hour and 75% remained intact at the 30th hour and 45% at the end of 72nd hour.

4. RESULTS AND DISCUSSION

4.1. Synthesis and Characterization of PLA

PLA is produced through a ring-opening polymerization (ROP) reaction, where the cyclic form of lactide undergoes polymerization according to literature protocol [71]. The catalyst $Sn(oct)_2$ binds to the ester carbonyl group of lactide, enhancing its reactivity. The BnOH molecule then attacks the carbonyl carbon, leading to the opening of the lactide ring and the formation of the PLA polymer chain. In essence, ROP of lactide to produce PLA entails the cleavage of the cyclic structure of lactide and the creation of a linear polymer chain composed of repeating lactide units. (Figure 4.1)

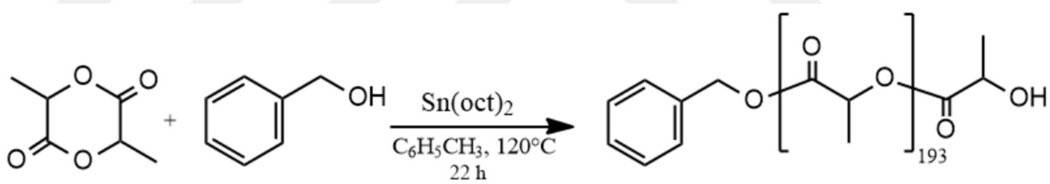

Figure 4.1. Synthesis of PLA.

Characterization of PLA block was done by ^{1}H NMR spectroscopy [72] (Figure 4.2). The number of lactide repeating units was determined by comparing the integration of the aromatic proton signals, which served as the reference point for BnOH around 7.4 ppm, with the integration of the proton signals at 5.2 ppm corresponding to the lactide moiety. This analysis revealed the presence of 193 lactide repeating units in the first block, calculated molecular weight 14.07 kDa. Furthermore, the molecular weight (Mn) of the PLA was found to be 15.54 kDa, and the polydispersity index (PDI) was determined to be 1.49 based on the GPC analysis.

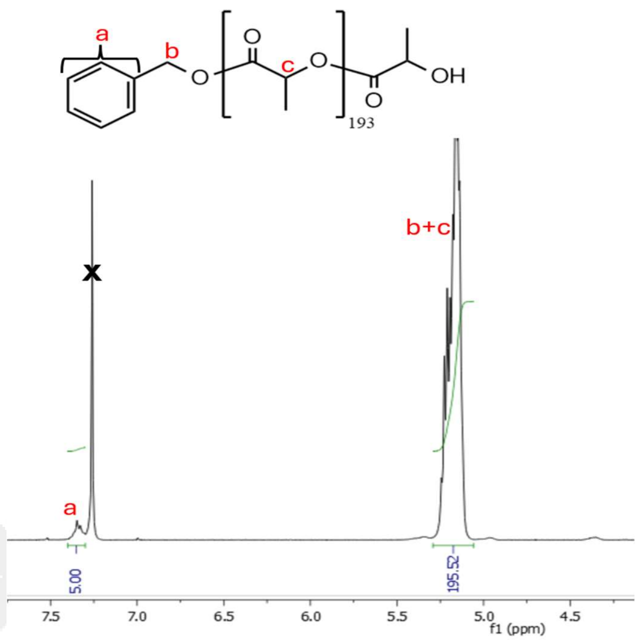

Figure 4.2. ^{1}H NMR spectrum of PLA.

4.2. Synthesis and Characterization of PCL

The synthesis of PCL from the cyclic monomer caprolactone also involves ROP process, as reported in the literature [73]. During this reaction, the caprolactone monomers undergo a cyclic opening process, which leads to the formation of linear PCL chains (Figure 4.3.). The reaction mechanism, including the use of alcohol, catalyst, and solvent, is quite similar to the synthesis of PLA.

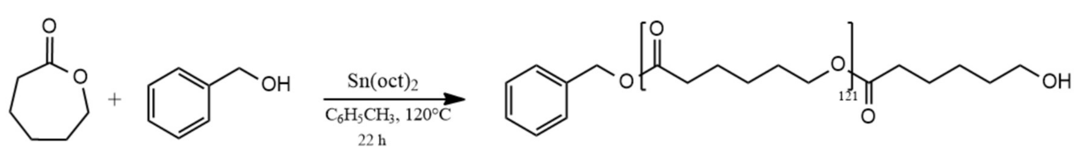

Figure 4.3. Synthesis of PCL.

The PCL block was characterized using ^{1}H NMR spectroscopy (Figure 4.4.). The analysis revealed that the PCL block contained 121 caprolactone repeating units, corresponding to a calculated molecular weight of 14.03 kDa. Additionally, Mn was determined to be 13.56 kDa, and the PDI was found to be 1.64 based on the GPC analysis.

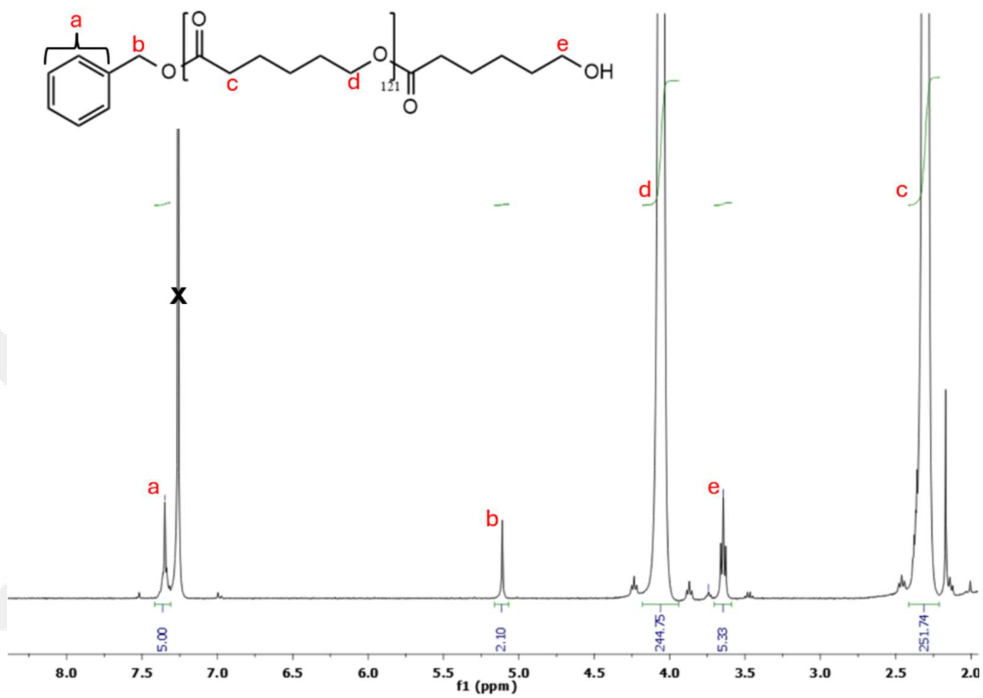

Figure 4.4. ^{1}H NMR spectrum of PCL.

4.3. Synthesis and Characterization of Macro Initiator PLA-CTA and PCL-CTA

A coupling reaction between DCC and DMAP is employed to facilitate the esterification of PLA or PCL with the carboxylate group of the CPADB, whereby DCC activates the CPADB's carboxylic acid group. This process allows the esterification of alcohol groups on first block with carboxylate groups of CPADB. Due to the formation of the ester linkage and synthesis of macro chain transfer agents, the second block can be grown on the polymer PLA- CTA (Figure 4.5) or PCL- CTA (Figure 4.6).

In the synthesis of macro initiator from first block polymer, the ratios of PLA (or PCL), CTA, DMAP and DCC were kept constant (1:4:0.8:4) for both reaction. Although both PLA-CTA were synthesized from the same PLA polymer, the decrease in solvent ratio increased the molecular weight of the polymer chain formed.

The synthesis of PCL- CTA was conducted using the same conditions employed in the synthesis of PLA- CTA, but the concentration was maintained at a higher level.

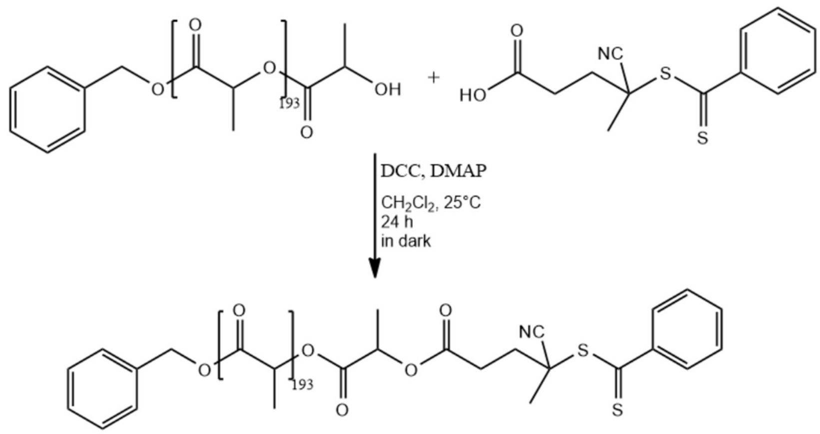

Figure 4.5. Synthesis of macro initiator agent PLA-CTA.

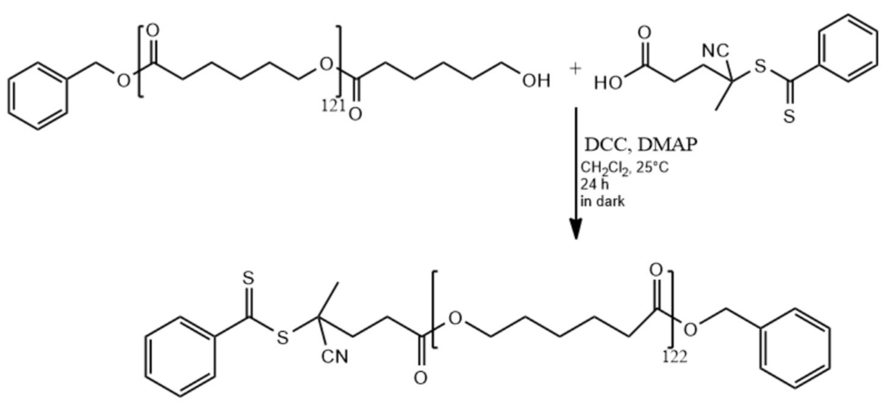

Figure 4.6. Synthesis of macro initiator agent PCL-CTA.

The successful synthesis of macroinitiators is verified by the presence of proton signals in ^{1}H NMR spectra. The aromatic protons of CPADB 's can be identified in the chemical shift range of 7.36 to 7.88 ppm. (Figure 4.7) Furthermore, when CPADB binds to PCL, the adjacent proton of the free OH group, represented by the 3.6 ppm peak, disappears (Figure 4.8).

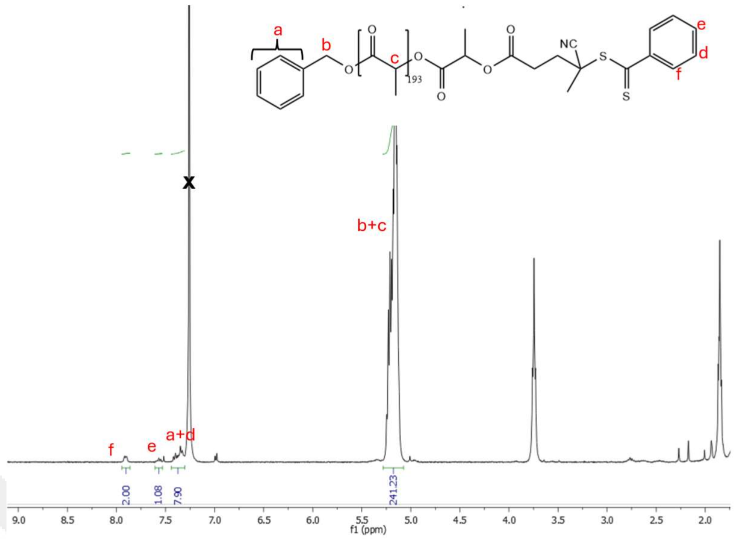

Figure 4.7. ^{1}H NMR spectrum of PLA- CTA.

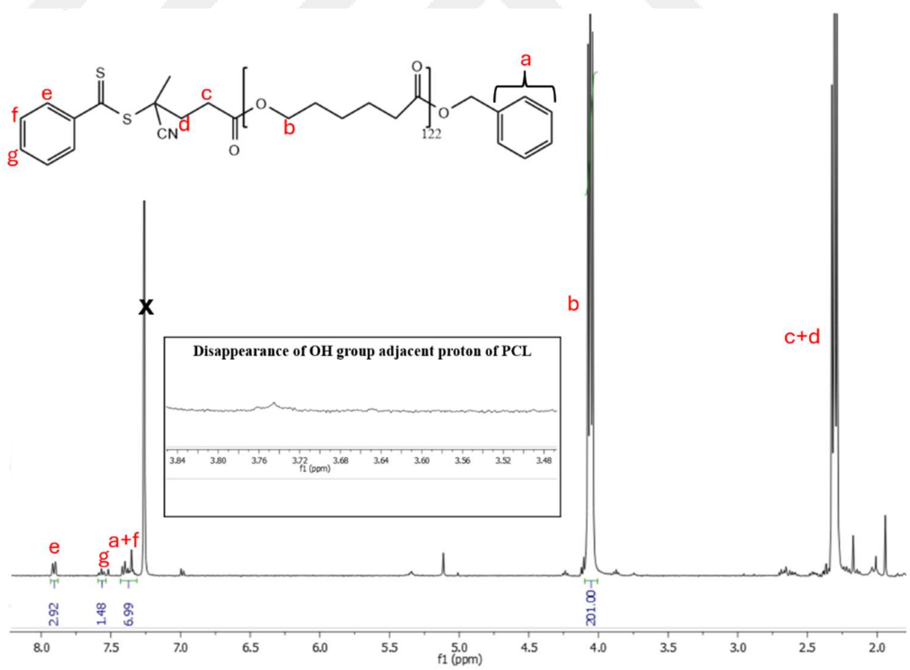

Figure 4.8. ^{1}H NMR spectrum of PCL- CTA.

4.4. Synthesis and Characterization of Diblock Polymer PLA-b-p(OEGMEMA) and PCL-b-p(OEGMEMA)

Block copolymers PLA-b-p(OEGMEMA) (Figure 4.9) and PCL-b-p(OEGMEMA) (Figure 4.10) were synthesized using RAFT polymerization, where OEGMEMA monomers were used to build the second block. The RAFT process employs the CPADB end of the macro initiator to regulate the growth of the polymer chains, resulting in well-defined polymer structures. The inclusion of the first block, formed by PLA or PCL, into the polymerization system facilitated the formation of block copolymers. The key functional group involved in RAFT polymerization is the thiocarbonylthio group of the CPADB, which undergoes a reversible addition-fragmentation process to control the growth of the polymer chains. The growth of polymers between the parts of the CPADB molecule is a consequence of the mechanism of RAFT polymerization. This process enables the creation of well-defined polymer structures with controlled molecular weights. The reaction resulted in 70% yield.

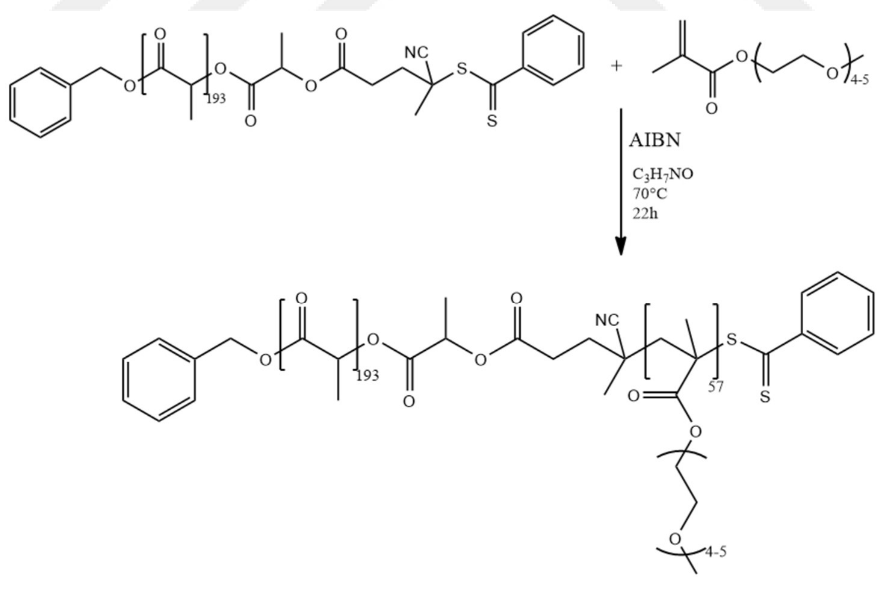

Figure 4.9. Synthesis of diblock PLA-b-p(OGMEMA).

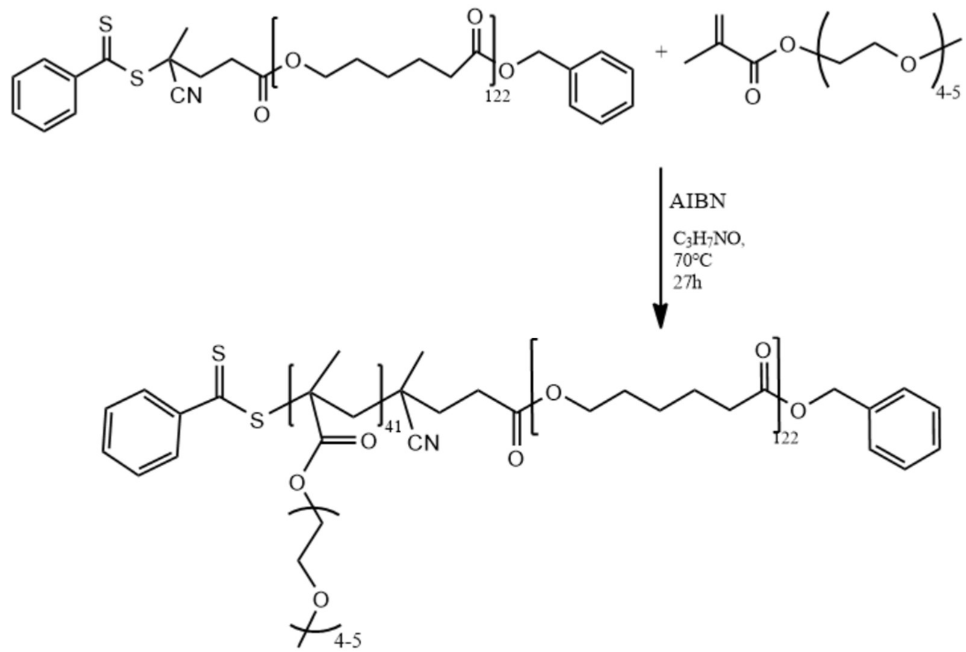

Figure 4.10. Synthesis of diblock PCL-b-p(OGMEMA).

The synthesized diblock polymers were analyzed using ^{1}H NMR spectroscopy. The appearance of proton signals around 3.37 ppm in both spectra, corresponding to the methyl ether terminal groups of the OEGMEMA monomer, confirmed that the polymerization process was successful in both instances. The signals of the initial blocks are used as a reference to determine the ratios and weights of the block polymers. The OEGMEMA repeating unit was 57 for PLA-b-p(OEGMEMA) and 41 for PCL-b-p(OEGMEMA), with calculated molecular weights of 31.17 kDa and 26.33 kDa, respectively. The Mn and PDI values obtained from GPC are 32.51 kDa, 1.43 and 25.13 kDa, 1.45, respectively.

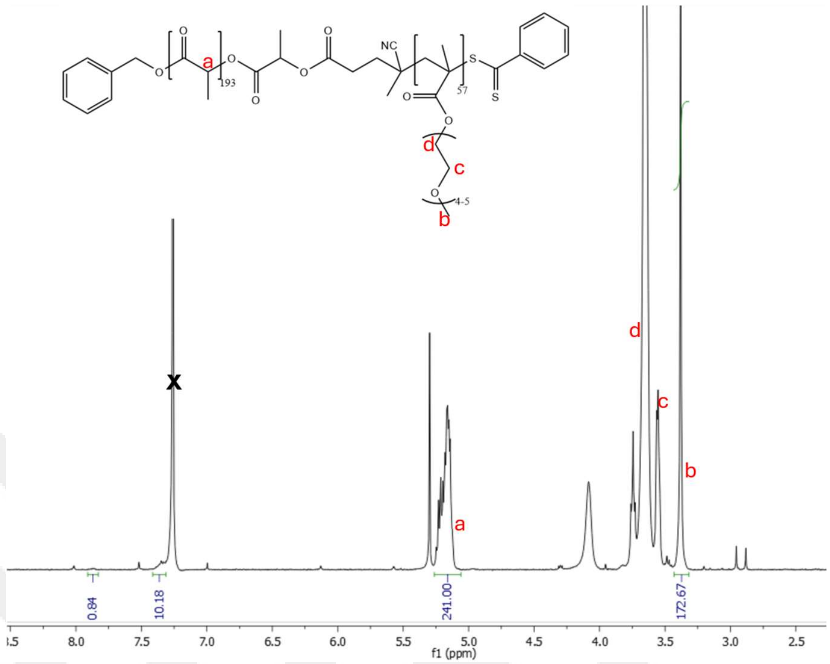

Figure 4.11. ^{1}H NMR spectrum of PLA-b-p(OEGMEMA).

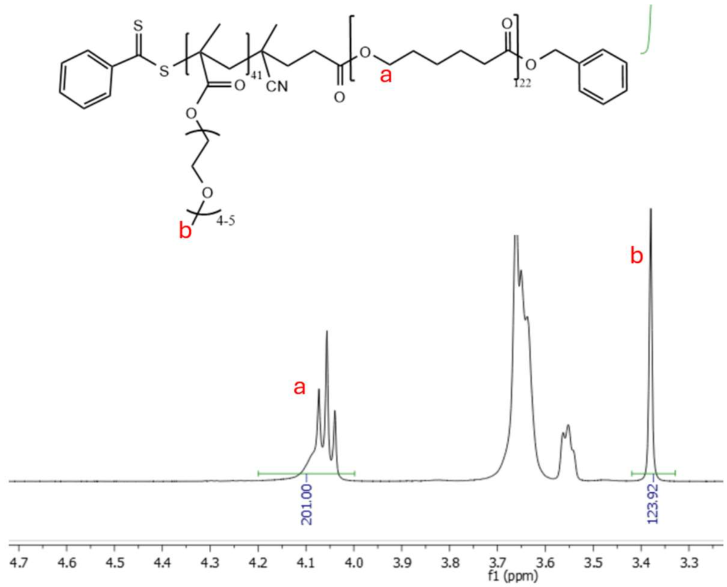

Figure 4.12. ^{1}H NMR spectrum of PCL-b-p(OEGMEMA).

Table 4.1. Repeating unit numbers and molecular weight values of synthesized polymers.

	M_1 Repeating Unit	M_2 Repeating Unit	Mn* (kDa)	Obtained Ratio M_1/M_2	Mn** (kDa)	PDI**
PLA	193	-	14.07	-	15.54	1.49
PCL	121	-	14.03	-	13.56	1.64
PLA-b-p(OEGMEMA)	193	57	31.17	1/1.2	32.51	1.43
PCL-b-p(OEGMEMA)	121	41	26.33	1/0.9	25.13	1.45

M_1: first block (PLA or PCL), M_2: p(OEGMEMA)

* Calculated using the ^{1}H-NMR proton resonance integration values
** Obtained by GPC using poly(methyl methacrylate) standards.

4.5. Critical Micelle Concentration (CMC) of Diblock Copolymers

CMC is the minimum concentration of a polymer required for it to self-assemble into micelles in an aqueous solution. This concept is commonly used to investigate the self-assembly behavior of amphiphilic polymers, as changes in the emission spectrum of the fluorescent probe, pyrene, can provide valuable insights into the formation and characteristics of the polymer micelles. To determine the CMC of the polymers, pyrene was employed as the fluorescence probe. Various samples were prepared by mixing the block polymer PLA-b-p(OEGMEMA) with pyrene in THF, adding water, and then evaporating the THF overnight. During the evaporation of the organic solvent, micelles begin to form if the concentration of the polymers exceeds the CMC value. The hydrophobic dye (pyrene) remaining in the aqueous solution migrates into the hydrophobic core of the micelles formed by the polymer, where it can dissolve and become visible. This transfer of the dye from the aqueous phase to the micelle core results in a significant change in the I_{338}/I_{334} ratio of pyrene, which is used to calculate the CMC value.

The CMC value is determined by identifying the intersection of the trendlines of the intensity ratios that are relatively constant and those that are rapidly increasing. The CMC values for two different block polymers were determined through experimental analysis. For the PLA-b-p(OEGMEMA) block copolymer, the CMC value was calculated to be 1.27 x

10^{-7}M, as illustrated in Figure 4.13. Similarly, for the PCL-b-p(OEGMEMA) block copolymer, the CMC value was calculated to be 1.08 x 10^{-7}M, as shown in Figure 4.14. These findings provide valuable insights into the self-assembly behavior and potential applications of these amphiphilic block copolymers. Since PLA-b-p(OEGMEMA) and PCL-b-p(OEGMEMA) had similar OEGMEMA repeating units and molecular weights, their CMC values were veritable as well.

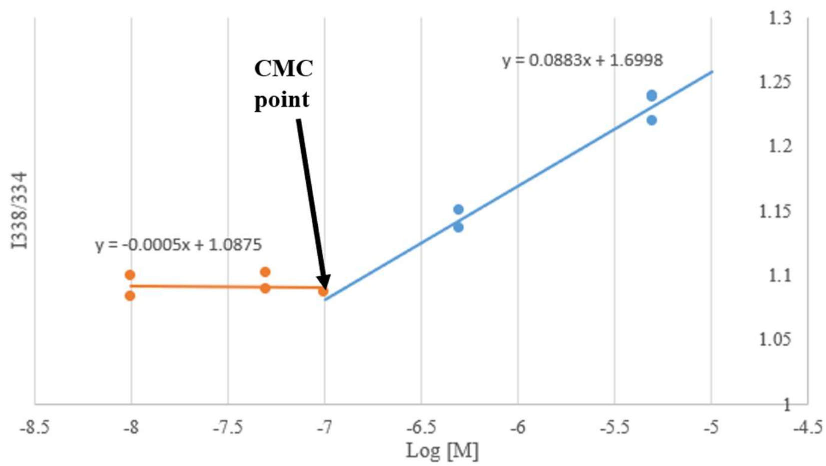

Figure 4.13. CMC graph of PLA-b-p(OEGMEMA) (1.27 x 10^{-7} M).

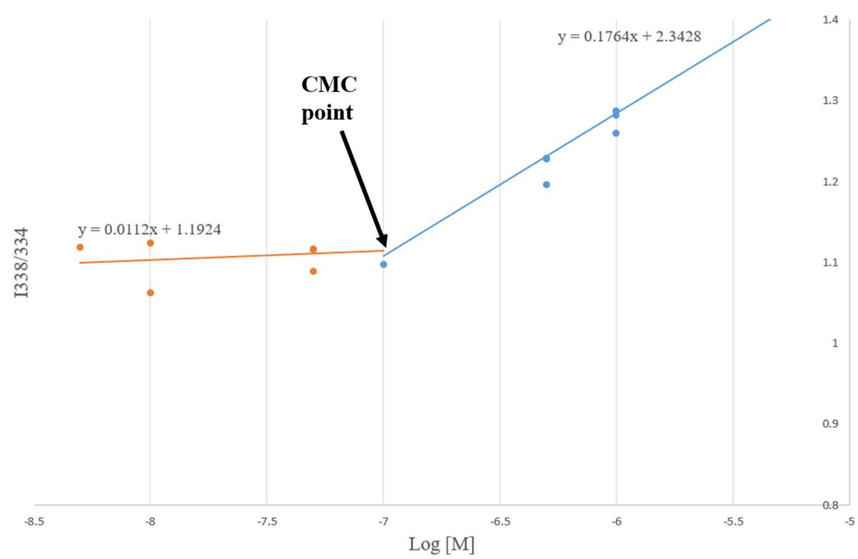

Figure 4.14. CMC graph of PCL-b-p(OEGMEMA) (1.08 x 10^{-7} M).

4.6. Formation of Polymeric Micelle

Amphiphilic polymers, which contain both hydrophobic (water-repelling) and hydrophilic (water-attracting) components within the same molecule, self-assemble in aqueous solutions to form micelles. When these polymers are placed in water, the hydrophobic parts tend to cluster together to minimize contact with water, while the hydrophilic parts interact with water molecules. This process leads to the formation of spherical structures called micelles, where the hydrophobic parts are sequestered in the core and the hydrophilic parts face outward, interacting with the surrounding solvent. The formation of micelles is driven by the hydrophobic effect, a thermodynamic phenomenon in which the entropy of the surrounding solvent increases as the hydrophobic moieties are sequestered in the core. This process is also influenced by factors such as temperature, polymer concentration, and the chemical nature of the polymer.

In the case of micellar nanoparticles, cosolvent evaporation was used to encapsulate dexamethasone within the hydrophobic core of the polymer-based micelles. This was achieved by dissolving the polymer and dexamethasone in THF and then adding distilled water dropwise to the mixture. After the organic solvent was evaporated, the drug molecules were trapped within the hydrophobic core of the micelles, PLA-b-p(OEGMEMA) and PCL-b-p(OEGMEMA).

In order to measure the size and PDI of the nanoparticle formed, DLS samples were prepared, and the nanoparticle was loaded with drug. LC-MS sample was prepared for the quantification of the drug loaded on the nanoparticle and analyzed by tenfold dilution. The size of the 5/10/15 wt.% dexamethasone loaded PLA-b-p(OEGMEMA) micelles and 5/10 wt.% dexamethasone loaded PCL-b-p(OEGMEMA) micelles were measured, shown in Table 4.2. The encapsulation efficiency (EE) of dexamethasone in micelles was found to be 94.8±0.03 for PLA-b-p(OEGMEMA) and 90.8±0.05 for PCL-b-p(OEGMEMA).

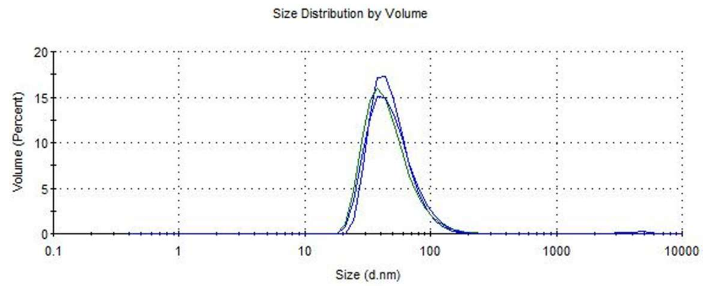

Figure 4.15. Size distributions of 5 wt% dexamethasone loaded PLA-b-p(OEGMEMA) micelles by volume.

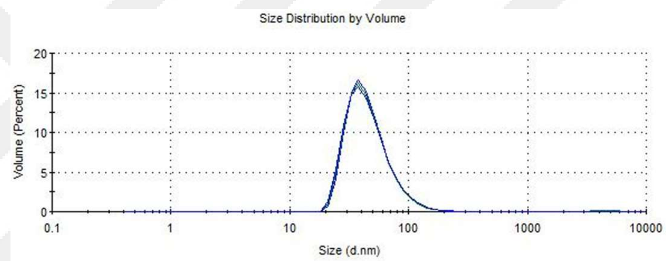

Figure 4.16. Size distributions of 10 wt% dexamethasone loaded PLA-b-p(OEGMEMA) micelles by volume.

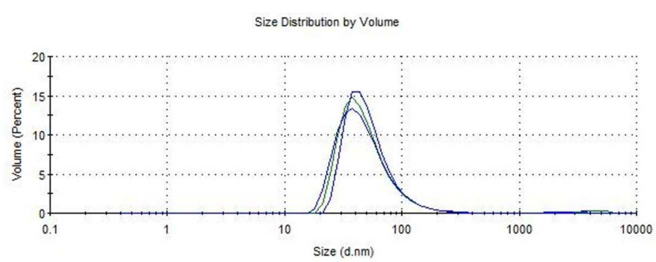

Figure 4.17. Size distributions of 15 wt% dexamethasone loaded PLA-b-p(OEGMEMA) micelles by volume.

Table 4.2. Average sizes and PDI values of all micellar nanoparticles.

	Drug Loading (wt%)	Average Size by Volume (nm)*	PDI*
PLA-b-p(OEGMEMA)	5	64.26	0.170
PLA-b-p(OEGMEMA)	10	64.35	0.193
PLA-b-p(OEGMEMA)	15	74.72	0.221
PCL-b-p(OEGMEMA)	5	68.01	0.190
PCL-b-p(OEGMEMA)	10	95.93	0.202

* Obtained by DLS measurements

4.7. Stability of Polymeric Micelles

The stability of polymeric micelles at upon ultra-dilution is an important consideration because the micelles undergo similar dilutions when injected into the inner ear fluids. Nanoparticles containing 1 x 10^{-5} M diblock polymer were prepared and micelle solutions were then diluted by a factor of two each time. The purpose was to observe the dilution factor up to which the micelles remain intact.

Volume based size change and the ratio of the PLA-b-p(OEGMEMA) nanoparticles in overall particulates were measured using DLS. The nanoparticle size, which did not change until 512-fold dilution with water, increased from 150 nm to 175 nm at 512-fold dilution. The size of the nanoparticles was not affected by the serial dilution with water up to a dilution of 2048 times. (Figure 4.18) However, the ratio of nanoparticles to total particles began to decrease dramatically at 256-fold dilution. This was due to the dissociation of the nanoparticles. In the case of serial dilution, irregular aggregate formation is possible. We have observed that the main reason for the decrease in the ratio of nanoparticles at serial dilution is due to the formation of such irregular aggregates. A similar stability behavior was also observed for PCL-b-p(OEGMEMA) particles by upon ultra-dilution studies (Figure 4.19).

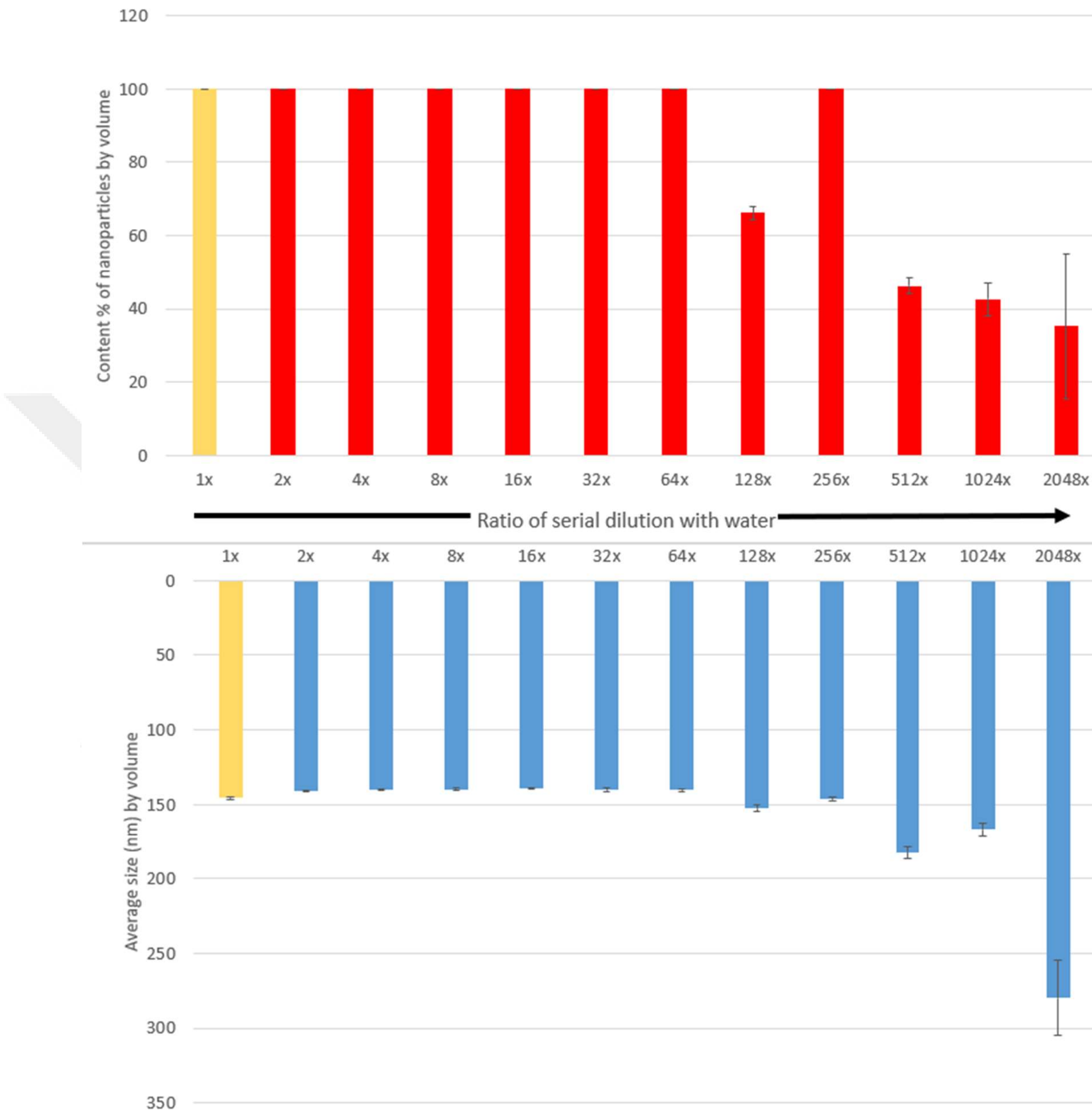

Figure 4.18. Stability of nanoparticle PLA-b-p(OEGMEMA) upon ultra-dilution with water.

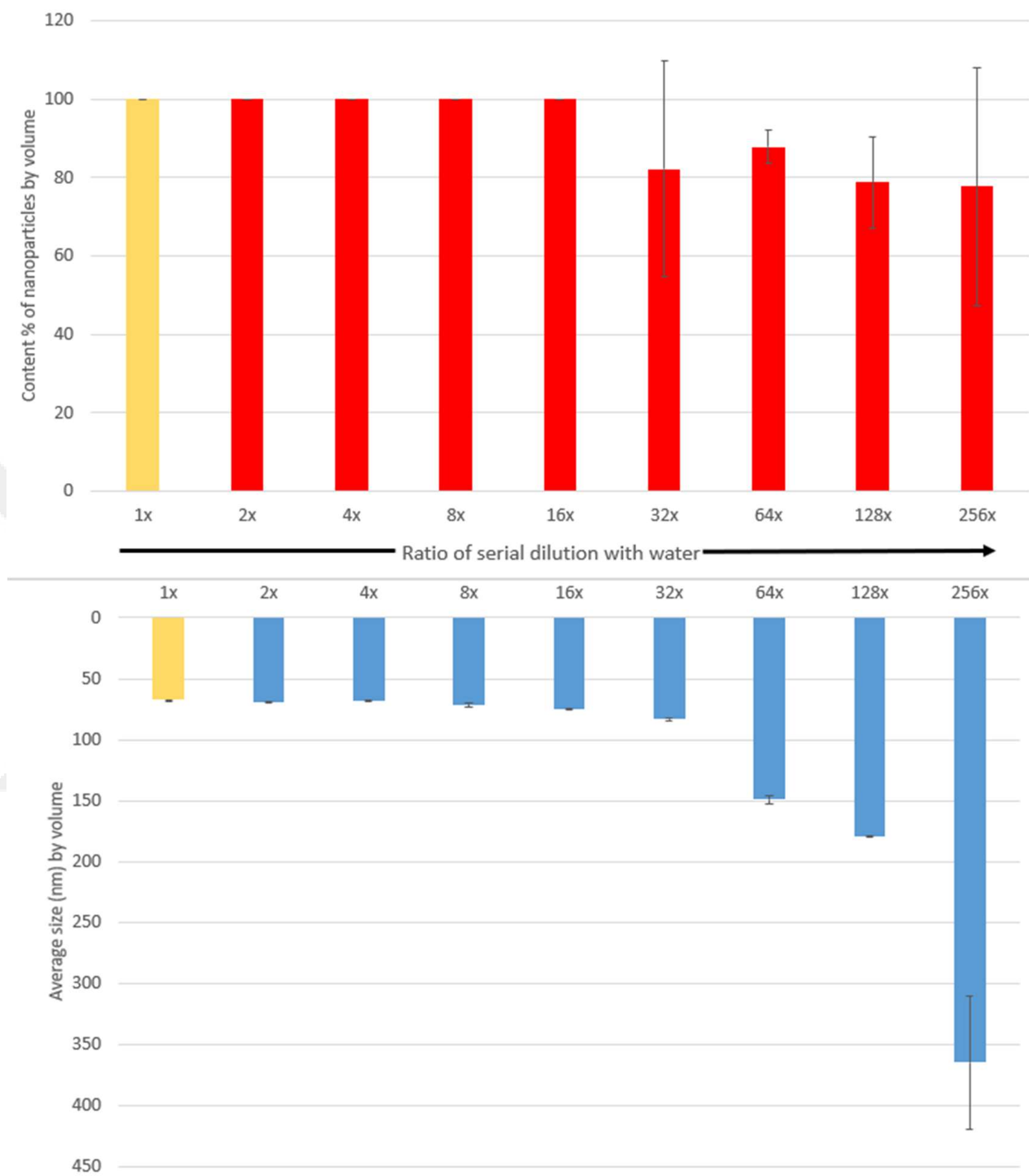

Figure 4.19. Stability of nanoparticle PCL-b-p(OEGMEMA) upon ultra-dilution with water.

4.8. *In vitro* Drug Release from Polymeric Micelles

The diblock polymers can be used as an effective delivery vehicle for the drug molecule of dexamethasone. The release kinetics were shown figures in different buffer solutions, including PBS, a-EL and a-PL, were all maintained at a physiologically relevant pH of 7.4.

The specific numerical data points may vary depending on the changes made to the concentrations and buffer solutions used. However, the general trend or profile of the drug release remains the same regardless of these alterations. To conduct an analysis, nanoparticles constructed from both PLA-b-p(OEGMEMA) and PCL-b-p(OEGMEMA) diblock polymers attain their peak release values within the initial 8 hours. Interestingly, the rate of drug release from these nanoparticles was faster than the sustained release patterns that have been reported in scientific publications on this topic.

PLA-b-p(OEGMEMA) nanoparticles containing 1/5/10 wt.% of dexamethasone were prepared, and the drug release was monitored for the first 8 hours in PBS buffer. As shown in Figure 4.20, the 1 wt% drug loaded micelle releases the drug at the slowest rate, while the 10 wt% drug loaded micelle releases the drug at the fastest rate. As the drug concentration increases in nanoparticles, more drug molecules are available to diffuse out of the matrix, leading to a higher release rate and speed. At the end of 8 hours, this sample has released over 90% of the drug while the other appears to have barely reached over 70%.

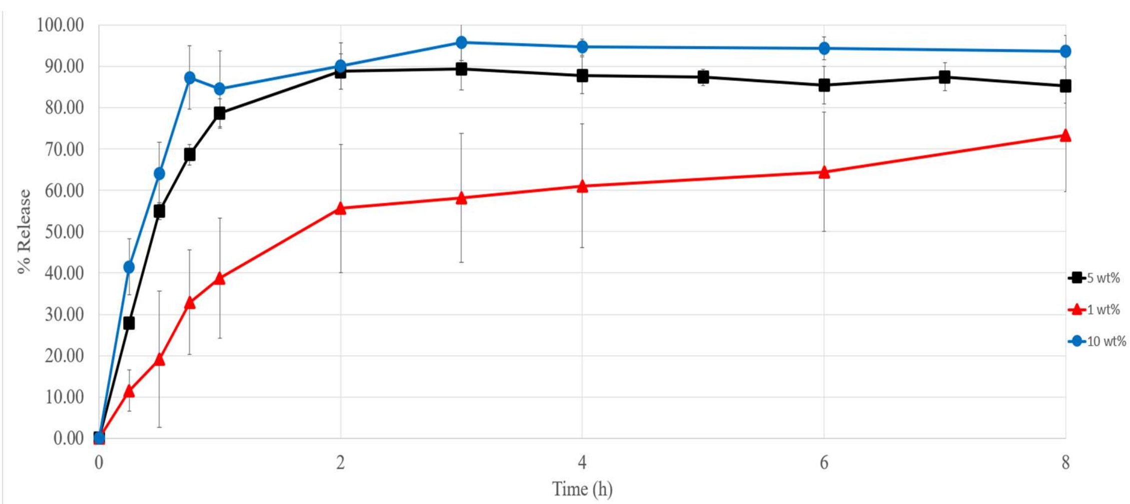

Figure 4.20. Release of dexamethasone from PLA-b-p(OEGMEMA) in PBS (●: 10 wt%, ▲: 1 wt%, ■ :5 wt%, dexamethasone loaded).

Since 1 wt% drug-loaded micelles consumed too much polymer and there was no significant difference in the drug release profile at the end of 8 h, the experiments were continued with 5 wt% drug-loaded micelles.

PLA-b-p(OEGMEMA) nanoparticle containing 5 wt% dexamethasone was prepared, and drug release was monitored in PBS, a-EL and a-PL buffer for the first 8 hours.

Since the ion concentrations of these three different buffer solutions are not very different from each other and they are all salt buffers, we can see that the drug release profiles are similar at Figure 4.21.

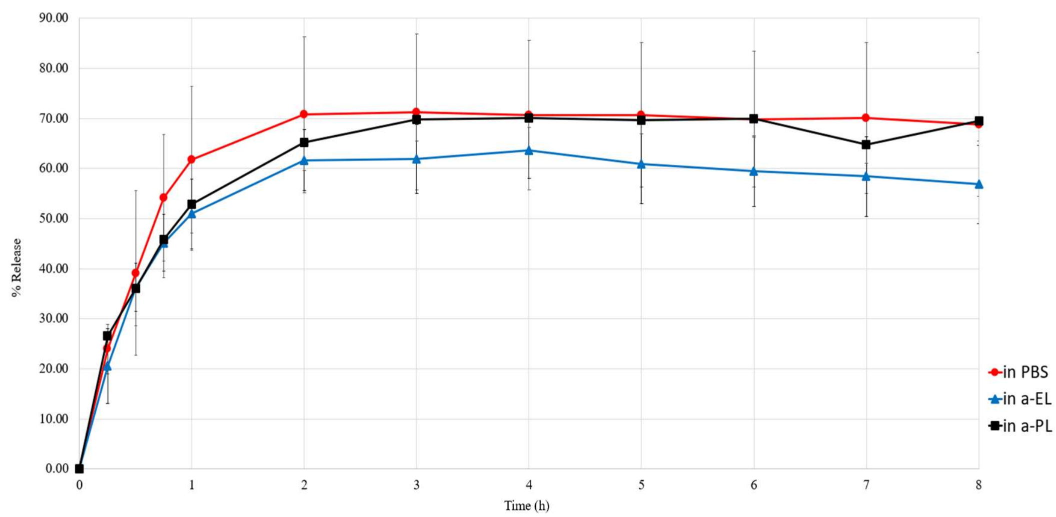

Figure 4.21. Release of dexamethasone from PLA-b-p(OEGMEMA) in different buffer solutions (●: in PBS, ■ :in a-PL, ▲:in a-EL buffer).

The initial results indicated that the release of a drug from a micelle system did not exceed 70% after 8 hours of observation at the end of 8 hours in Figure 4.21, suggesting that a significant portion of the drug remained trapped within the micelle structure. To address this issue, the effect of reducing the buffer ion concentration was investigated to experiment release of dexamethasone from PLA-b-p(OEGMEMA) in a-EL buffer.

By diluting the buffer solution by 2-fold and 4-fold, the aim was to lower the ion concentrations and potentially improve drug release. The results showed that the 4-fold dilution of the buffer concentration resulted in an increase in drug release from 70% to 90%, as shown in Figure 4.22. This suggests that the initial high ion concentration of the buffer solution was a limiting factor in the complete release of the drug from the micelle.

It is concluded that the fact that not all the dexamethasone was released from the micelle can be interpreted as an indication that the ionic concentration of the buffer was too high, which hindered the complete extraction of the drug. This finding highlights the importance of optimizing buffer conditions to achieve more efficient drug release from the micelle system.

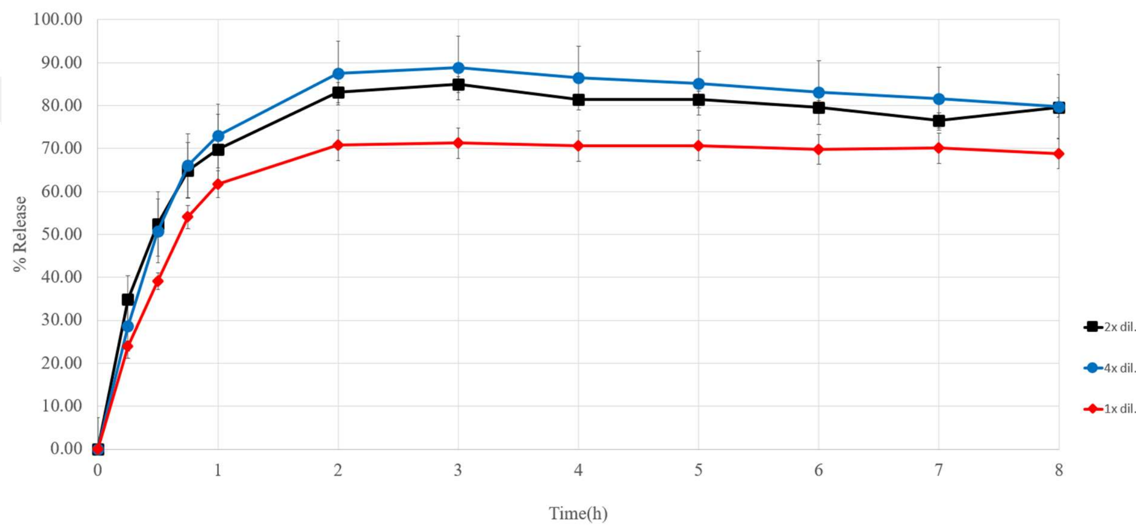

Figure 4.22. Release of dexamethasone from PLA-b-p(OEGMEMA) in a-EL buffer with different concentration (●:4x diluted, ■ :2x diluted, ▲: 1x buffer).

Nanoparticles were prepared from two different block copolymers, PLA-b-p(OEGMEMA) and PCL-b-p(OEGMEMA), both containing 5 wt.% of the drug dexamethasone. Drug release from these nanoparticles was monitored over the first 8 hours in an a-EL buffer solution. As shown in Figure 4.23, the drug release profiles of the two types of nanoparticles were quite comparable. This similarity in drug release behavior can be attributed to the comparable molecular weights of the two block copolymers, which were 34 kDa and 24 kDa, respectively. In addition, the ratio of hydrophobic to hydrophilic blocks was 1:1 for both copolymers, which further contributed to the analogous drug release patterns observed. It is likely that the pairing of the hydrophobic and hydrophilic blocks in these block copolymers played a key role in facilitating the controlled and sustained release of the dexamethasone from the nanoparticle formulations.

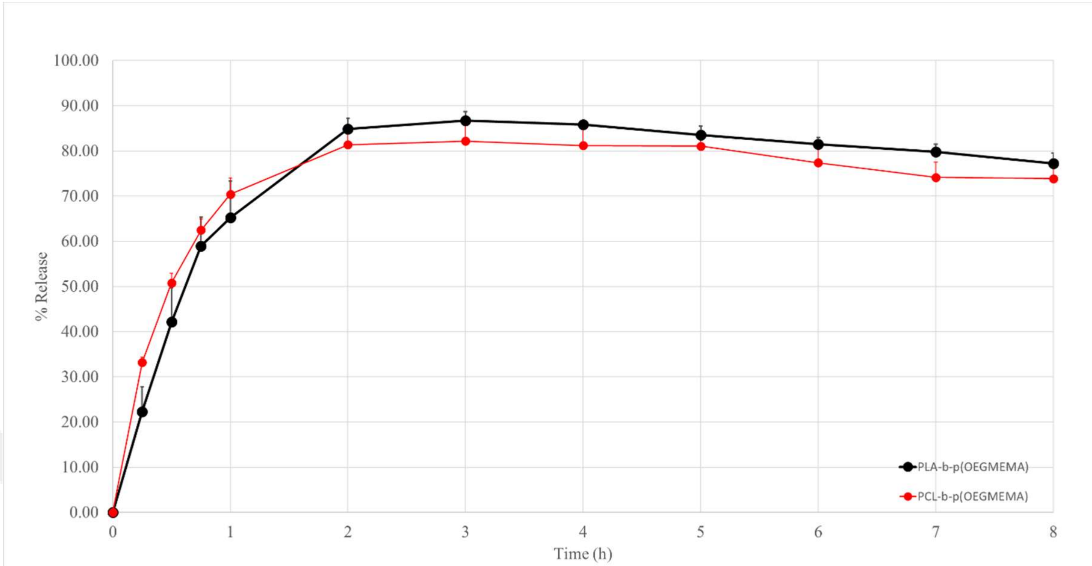

Figure 4.23. Release of 5 wt% dexamethasone loaded PLA-b-p(OEGMEMA) (black line) and PCL-b-p(OEGMEMA) (red line) in a-EL.

5. CONCLUSION

In this research project, a nanoparticle system was developed as a potential drug delivery vehicle for hair cells within the inner ear cochlea. The nanoparticle consisted of an amphiphilic polymer, which is a type of material that possesses both hydrophilic and hydrophobic properties. PLA was selected due to its biodegradability, meaning it can be broken down without causing harm to the environment. Additionally, PLA is known to be non-toxic, making it a safe option for various biomedical applications. For desired diblock copolymer structure, the initial polymer blocks of PLA and PCL were synthesized using ROP technique. Then, a chain transfer agent, CPADB, was attached to the initial blocks, allowing for the growth of a second polymer block. The second blocks were grown on the first blocks by RAFT polymerization to obtain diblock polymers PLA-b-p(OEGMEMA) and PCL-b-p(OEGMEMA). These amphiphilic polymers were used to prepare polymeric micelles. Their size, drug loading and stability were determined. The size, drug loading capacity, and stability of the prepared micelles were thoroughly characterized. It was found that the similar molecular weights and block ratios of the polymers led to comparable micelle sizes, CMC values, and drug release profiles. The drug-loaded micelles, which contained approximately 5 wt% dexamethasone, were observed to have an average size of 60-70 nm and exhibited quite stability against upon dilution. *In vitro* drug release studies, the release kinetics of the drug from the micelles were investigated in different buffer solutions, including PBS, a-EL, and a-PL. The results showed that the drug release ranged from 60% to 70% within the first 8 hours, with the release rate increasing as the buffer concentration decreased and decreasing as the drug loading percentage decreased. Notably, release profiles of the PLA-b-p(OEGMEMA) and PCL-b-p(OEGMEMA) were compared and exhibited similar drug release profiles in the a-EL buffer at a 5% dexamethasone loading. Future work may include envisioning the potential to further functionalize these diblock copolymers by incorporating additional linkers or moieties onto the polymer chains. This could enable enhanced drug delivery and potentially slow down the drug release rate, ultimately improving the therapeutic efficacy of the nanoparticle-based drug delivery system for hair cell-related disorders in the inner ear cochlea.

REFERENCES

1. Sheikh, A., B. Zainab, K. Shabbir, and A. Imtiaz, *Auditory System, Function and Disorders*, SPRINGER NEW YORK, London, 2022.

2. National Institute on Deafness and Other Communication Disorders, “How Do We Hear?”, 2022, https://www.nidcd.nih.gov/health/how-do-we-hear, accessed on May 8 2024.

3. Moore, B. C. J., *An Introduction to the Psychology of Hearing*. 6th edition, BRILL, Boston, 2013.

4. Wilson, J.P., and D. T. Kemp, *Springer Science & Business Media*, 1st edition, SPRINGER, Newyork, 2012.

5. Duvall, A. J., and V. T. Rhodes, “Reissner’s Membrane: an Ultrastructural Study”, *Archives of Otolaryngology-Head and Neck Surgery,* Vol. 86, No.2, pp. 143–151, 1967.

6. Kimura, R. S. , “The Ultrastructure of the Organ of Corti”. *In International Review of Cytology* pp. 173–222, 1975.

7. Tona, R., I. A. López, C. Fenollar–Ferrer, R. Faridi, C. Anselmi, A. A. Khan, M. Shahzad, R. J. Morell, S. Gu, M. Hoa, L. Dong, A. Ishiyama, I. A. Belyantseva, S. Riazuddin, and T. B. Friedman, “Mouse Models of Human Pathogenic Variants of TBC1D24 Associated with Non-Syndromic Deafness DFNB86 and DFNA65 and Syndromes Involving Deafness”, *Genes*, Vol. 11, No. 10, p. 1122, 2020.

8. Frolenkov, G. I., I. A. Belyantseva, T. B. Friedman, and A. J. Griffith, “Genetic Insights into the Morphogenesis of Inner Ear Hair Cells”, *Nature Reviews. Genetics*, Vol. 5, No. 7, pp. 489–498, 2004.

9. Frolenkov, G. I., M. Atzori, F. Kalinec, F. Mammano, and B. Kachar, " The Membrane-Based Mechanism of Cell Motility in Cochlear Outer Hair Cells", *Molecular Biology of the Cell*, Vol. 9, No. 8, pp. 1961–1968, 1998.

10. Wagner, E., and J. Shin, " Mechanisms of Hair Cell Damage and Repair", Trends in Neurosciences, Vol. 42, No. 6, pp. 414–424, 2019.

11. Vos, T., A. A. Abajobir, K. H. Abate, C. Abbafati, K. Abbas, F. Abd-Allah, R. S. Abdulkader, A. Abdulle, T. A. Abebo, S. F. Abera, V. Aboyans, L. J. Abu-Raddad, I. N. Ackerman, A. A. Adamu, O. Adetokunboh, M. Afarideh, A. Afshin, S. K. Agarwal, R. Aggarwal, and C. J. L. Murray, "Global, Regional, and National Incidence, Prevalence, and Years Lived with Disability for 328 Diseases and Injuries for 195 Countries, 1990–2016 : a Systematic Analysis for the Global Burden of Disease Study 2016", *Lancet*, Vol. 390, No. 10100, pp. 1211–1259, 2017.

12. World Health Organization (WHO), "Deafness and Hearing Loss", 2024, https://www.who.int/news-room/fact-sheets/detail/deafness-and-hearing-loss, accessed on May 9, 2024.

13. Cunningham, L. L., and D. L. Tucci, "Hearing Loss in Adults", *New England Journal of Medicine*, Vol. 377, No. 25, pp. 2465–2473, 2017.

14. Møller, A. R., B. Langguth, D. DeRidder, and T. Kleinjung, *Textbook of Tinnitus*, First Edition, Springer, New York, 2011.

15. Delmaghani, S., and A. El-Amraoui, "Inner Ear Gene Therapies Take Off: Current Promises and Future Challenges", *Journal of Clinical Medicine*, Vol. 9, No. 7, p. 2309, 2020.

16. Lp, R., A. Dhukhwa, D. Mukherjea, and V. Ramkumar, "Local Drug Delivery for Prevention of Hearing Loss", *Frontiers in Cellular Neuroscience*, Vol. 13, No.300, pp. 1-14, 2019.

17. Jahnke, K., “The Blood-Perilymph Barrier”, *Archives of Oto-Rhino-Laryngology*, Vol. 228, No. 1, pp. 29–34, 1980.

18. Nyberg, S., N.J. Abbott, X. Shi, P. S. Steyger, and A. Dabdoub, “Delivery of Therapeutics to the Inner Ear: The Challenge of the Blood-Labyrinth Barrier”, *Science Translational Medicine*, Vol. 11, No. 482, p. eaao0935, 2019.

19. An, X., and D. Zha, “Development of Nanoparticle Drug-Delivery Systems for the Inner Ear”, Nanomedicine, Vol. 15, No. 20, pp. 1981–1993, 2020.

20. Buniel, M. C., K. Geelan-Hansen, P. Weber, and V. K. Tuohy, “Immunosuppressive Therapy for Autoimmune Inner Ear Disease”, *Immunotherapy*, Vol. 1, No. 3, pp. 425–434, 2009.

21. Jackson, L. E., and H. Silverstein, “Chemical Perfusion of the Inner Ear”, *Otolaryngologic Clinics of North America*, Vol. 35, No. 3, pp. 639–653, 2002.

22. Lehner, E., A. Liebau, F. Syrowatka, W. Knolle, S.K. Plontke, and K. Mäder, “Novel Biodegradable Round Window Disks for Inner Ear Delivery of Dexamethasone”, *International Journal of Pharmaceutics*, Vol. 594, p. 120180, 2021.

23. Hahn, H., B. Kammerer, A. DiMauro, A. N. Salt, and S. K. Plontke, “Cochlear Microdialysis for Quantification of Dexamethasone and Fluorescein Entry Into Scala Tympani During Round Window Administration”, *Hearing Research*, Vol. 212, No. 1-2, pp. 236-244, 2006.

24. Swan, E. E. L., M. J. Mescher, W. F. Sewell, S. L. Tao, and J. T. Borenstein, “Inner Ear Drug Delivery for Auditory Applications”, *Advanced Drug Delivery Reviews*, Vol. 60, No. 15, pp. 1583–1599, 2008.

25. Ikeda, K., and T. Morizono, “Round Window Membrane Permeability During Experimental Purulent Otitis Media: Altered Cortisporin Ototoxicity”, *Annals of Otology, Rhinology & Laryngology*, Vol. 99, No. 6_suppl, pp. 46–48, 1990.

26. Dash, S., J. Zuo, and P. S. Steyger, “Local Delivery of Therapeutics to the Cochlea Using Nanoparticles and Other Biomaterials”, *Pharmaceuticals*, Vol. 15, No. 9, p. 1115, 2022.

27. Jaudoin, C., F. Agnely, Y. Nguyen, E. Ferrary, and A. Bochot, “Nanocarriers for Drug Delivery to the Inner eEar: Physicochemical Key Parameters, Biodistribution, Safety and Efficacy”, *International Journal of Pharmaceutics*, Vol. 592, p. 120038, 2021.

28. Langer, R., and N. Peppas “Present and Future Applications of Biomaterials in Controlled Drug Delivery Systems”, *Biomaterials*, Vol. 2, No. 4, pp. 201–214, 1981.

29. Couvreur, P., “Nanoparticles in Drug Delivery: Past, Present and Future”, *Advanced Drug Delivery Reviews*, Vol. 65, No. 1, pp. 21–23, 2013.

30. Chen, G., X. Zhang, F. Yang, and L. Mu,” Disposition of Nanoparticle-Based Delivery System via Inner Ear Administration”, *Current Drug Metabolism*, Vol. 11, No. 10, pp. 886–897, 2010.

31. Buckiová, D., S. Ranjan, T. A. Newman, A. H. Johnston, R. Sood, P. K . Kinnunen, J. Popelář, T. Chumak, and J. Syka, “Minimally Invasive Drug Delivery to the Cochlea Through Application of Nanoparticles to the Round Window Membrane”, *Nanomedicine*, Vol. 7, No. 9, pp. 1339–1354, 2012.

32. Zou, J., P. Saulnier, T. Perrier, Y. Zhang, T. Manninen, E. Toppila, and I. Pyykkö, “Distribution of Lipid Nanocapsules in Different Cochlear Cell Populations After Round Window Membrane Permeation”, *Journal of Biomedical Materials Research Part B, Applied Biomaterials,* Vol. 87B, No. 1, pp. 10–18, 2008.

33. Mittal, R., S. Peña, A. Zhu, N. Eshraghi, A. Fesharaki, E. J. Horesh, J. Mittal, and A. A. Eshraghi, “Nanoparticle-based Drug Delivery in the Inner Ear: Current Challenges, Limitations and Opportunities”, *Artificial Cells, Nanomedicine, and Biotechnology*, Vol. 47, No. 1, pp. 1312–1320, 2019.

34. Wen, X., S. Ding, H. Cai, J. Wang, L. Wen, F. Yang, and G. Chen, "Nanomedicine Strategy for Optimizing Delivery to Outer Hair Cells by Surface-Modified poly(lactic/glycolic acid) Nanoparticles with Hydrophilic Molecules", *International Journal of Nanomedicine*, Vol. 11, pp. 5959–5969, 2016.

35. Huynh, N. T., C. Passirani, P. Saulnier, and J. Benoit, "Lipid Nanocapsules: A New Platform for Nanomedicine", *International Journal of Pharmaceutics*, Vol. 379, No. 2, pp. 201–209, 2009.

36. Singh, N., G. Jenkins, R. Asadi, and S. H. Doak, "Potential Toxicity of Superparamagnetic Iron Oxide Nanoparticles (SPION)", *Nano Reviews*, Vol. 1, No.1, p. 5358, 2010.

37. Musazzi, U. M., S. Franzè, and F. Cilurzo, "Innovative Pharmaceutical Approaches for the Management of Inner Ear Disorders", *Drug Delivery and Translational Research*, Vol. 8, No. 2, pp. 436–449, 2017.

38. Salt, A. N., and S. K. Plontke, "Pharmacokinetic Principles in the Inner Ear: Influence of Drug Properties on Intratympanic Applications", *Hearing Research*, Vol. 368, pp. 28–40, 2018.

39. King, E. B., A. N. Salt, H. Eastwood, and S. O'Leary, "Direct Entry of Gadolinium into the Vestibule Following Intratympanic Applications in Guinea Pigs and the Influence of Cochlear Implantation", *Journal of the Association for Research in Otolaryngology*, Vol. 12, No. 6, pp. 741–751, 2011.

40. Shi, X, "Pathophysiology of the cochlear intrastrial fluid-blood barrier", *Hearing Research*, Vol. 338, pp. 52-63, 2016.

41. Kechai, N. E., E. Mamelle, Y. Nguyen, N. Huang, V. Nicolas, P. Chaminade, S. Yen-Nicolaÿ, C. Gueutin, B. Granger, E. Ferrary, F. Agnely, and A. Bochot,"Hyaluronic

Acid Liposomal Gel Sustains Delivery of a Corticoid to the Inner Ear", *Journal of Controlled Release*, Vol. 226, pp. 248–257, 2016.

42. Rathnam, C., S. D. Chueng, Y. Yue, K. Lee, and K. Y. Kwan, "Developments in Bio-Inspired Nanomaterials for Therapeutic Delivery to Treat Hearing Loss", *Frontiers in Cellular Neuroscience*, Vol. 13, pp. 1-13 2019.

43. McCall, A. A., E. E. L. Swan, J. T. Borenstein, W. F. Sewell, S. G. Kujawa, and M. J. McKenna, "Drug Delivery for Treatment of Inner Ear Disease: Current State of Knowledge", *Ear and Hearing*, Vol. 31, No. 2, pp. 156–165, 2010.

44. Zhang, L., Y. Xu, W. Cao, S. Xie, L. Wen, and G. Chen, "Understanding the Translocation Mechanism of PLGA Nanoparticles Across Round Window Membrane into the Inner Ear: A Guideline for Inner Ear Drug Delivery Based on Nanomedicine", *International Journal of Nanomedicine*, Vol. 13, pp. 479–492, 2018.

45. Zlotnikov, I. D., A. A. Ezhov, A. S. Ferberg, С. С. Крылов, M. N. Semenova, В. В. Семенов, and E. V. Kudryashova, "Polymeric Micelles Formulation of Combretastatin Derivatives with Enhanced Solubility, Cytostatic Activity and Selectivity Against Cancer Cells", *Pharmaceutics*, Vol. 15, No. 6, p. 1613 ,2023.

46. Ghezzi, M., S. Pescina, C. Padula, P. Santi, E. DelFavero, and L. Cantù, "Polymeric Micelles in Drug Delivery: An Insight of the Techniques for Their Characterization and Assessment in Biorelevant Conditions", *Journal of Controlled Release*, Vol. 332, pp. 312–336, 2021.

47. Ashique, S., A. Garg, A. Hussain, S. Bhatt, A. Agrawal, and N. Mishra, "Polymeric Micelles in the Delivery of Proteins", *In Polymeric Micelles: Principle, Perspective and Practice*, pp. 231–251, 2023.

48. Lin, W., L. Juang, and C. Lin, "Stability and Release Performance of a Series of Pegylated Copolymeric Micelles", *Pharmaceutical Research*, Vol. 20, No. 4, pp. 668–673, 2003.

49. Trivedi, R., and U. B. Kompella, "Nanomicellar Formulations for Sustained Drug Delivery: Strategies and Underlying Principles", *Nanomedicine*, Vol. 5, No. 3, pp. 485–505, 2010.

50. Imran, M., M. R. Shah, and Shafiullah, "Amphiphilic Block Copolymers–Based Micelles for Drug Delivery", *Design and Development of New Nanocarriers*, pp. 365–400, 2018.

51. Owen, S. C., D. P. Chan, and M. S. Shoichet, "Polymeric Micelle Stability", *Nano Today*, Vol. 7, pp. 53–65, 2012.

52. Lee, J., E. C. Cho, and K. Cho, "Incorporation and Release Behavior of Hydrophobic Drug in Functionalized poly(d,l-lactide)-block–poly(ethylene oxide) Micelles", *Journal of Controlled Release*, Vol. 94, No. 2–3, pp. 323–335, 2004.

53. Lü, Y., E. Zhang, J. Yang, and Z. Cao, "Strategies to Improve Micelle Stability for Drug Delivery", *Nano Research*, Vol. 11, No. 10, pp. 4985–4998, 2018.

54. Phogat, N., M. Kohl, I. Uddin, and A. Jahan, "Interaction of Nanoparticles with Biomolecules, Protein, Enzymes, and Its Applications", *Precision Medicine*, pp. 253–276, 2018.

55. Zeng, L., J. Gao, Y. Liu, J. Gao, L. Yao, X. Yang, X. Liu, B. He, L. Hu, J. Shi, M. Song, G. Qu, and G. Jiang, "Role of Protein Corona in the Biological Effect of Nanomaterials: Investigating Methods", *TrAC Trends in Analytical Chemistry*, Vol. 118, pp. 303–314, 2019.

56. Chen, E. Y., W. F. Liu, L. Megido, P. Díez, M. Fuentes, C. Fager, E. Olsson, I. Gessner, and S. Mathur, "Understanding and Utilizing the Biomolecule/Nanosystems Interface", *Nanotechnologies in Preventive and Regenerative Medicine* , pp. 207–297, 2018.

57. Zhu, Y., T. Meng, Y. Tan, X. Yang, Y. Liu, X. Li, F. Yu, L. Wen, S. Dai, H. Yuan, and F. Hu, “Negative Surface Shielded Polymeric Micelles with Colloidal Stability for Intracellular Endosomal/Lysosomal Escape”, *Molecular Pharmaceutics*, Vol. 15, No. 11, pp. 5374–5386, 2018.

58. Diezi, T. A., Y. Bae, and G. S. Kwon, “Enhanced Stability of PEG-block-poly(N-hexyl stearate l-aspartamide) Micelles in the Presence of Serum Proteins”, Molecular Pharmaceutics, Vol. 7, No. 4, pp. 1355–1360, 2010.

59. Pepić, I., J. Lovrić, and J. Filipović-Grčic, “How Do Polymeric Micelles Cross Epithelial Barriers?”, *European Journal of Pharmaceutical Sciences*, Vol. 50, No. 1, pp. 42–55, 2013.

60. Grimaudo, M. A., S. Pescina, C. Padula, P. Santi, A. Concheiro, and C. Alvarez-Lorenzo, “Topical Application of Polymeric Nanomicelles in Ophthalmology: A Review on Research Efforts for the Noninvasive Delivery of Ocular Therapeutics”, *Expert Opinion on Drug Delivery*, Vol. 16, No. 4, pp. 397–413, 2019.

61. Zhou, Q., L. Zhang, T. Yang, and H. Wu, “Stimuli-Responsive Polymeric Micelles for Drug Delivery and Cancer Therapy”, *International Journal of Nanomedicine*, Vol. 13, pp. 2921–2942, 2018.

62. Koltzenburg, S., M. Maskos, and O. Nuyken, “Ring-Opening Polymerization”, *Polymer Chemistry*, pp. 321–347, 2017.

63. Nuyken, O., and S. D. Pask, “Ring-Opening Polymerization—An Introductory Review”. *Polymers*, Vol. 5, No. 2, pp. 361–403, 2013.

64. Duda, A., and A. Kowalski, “Thermodynamics and Kinetics of Ring-Opening Polymerization”, *Handbook Ring - Opening Polymerization*, pp. 1–51, 2009.

65. Perrier, S. “50th Anniversary Perspective: RAFT Polymerization—A User Guide”, *Macromolecules*, Vol. 50, No. 19, pp. 7433–7447, 2017.

66. Lei, T., J. Liu, J. Xu, and T. P. Davis, “Synthesis and Bioactivity of poly(HPMA)–lysozyme Conjugates: The Use of Novel thiazolidine-2-thione Coupling Chemistry”, *Organic & Biomolecular Chemistry*, Vol. 7, No. 17, p. 3481, 2009.

67. Fairbanks, B. D., P. A. Gunatillake, and L. Meagher, “Biomedical Applications of Polymers Derived by Reversible Addition – Fragmentation Chain-Transfer (RAFT)”, Advanced Drug Delivery Reviews, Vol. 91, pp.141–152, 2015.

68. Smith, P. P., and S. G. Boyes, “Synthesis of Amphiphilic Block Copolymers via Ring Opening Polymerization and Reversible Addition-Fragmentation Chain Transfer Polymerization”, *Journal of Polymer Science*, Vol. 59, No.1, pp. 43–58, 2020.

69. Keddie, D. J. “A guide to the Synthesis of Block Copolymers Using Reversible-Addition Fragmentation Chain Transfer (RAFT) Polymerization”, *Chemical Society Reviews*, Vol. 43, No. 2, pp. 496–505, 2014.

70. Wangemann, P. “Supporting Sensory Transduction: Cochlear Fluid Homeostasis and the Endocochlear Potential”, *The Journal of Physiology*, Vol. 576, No.1, pp. 11–21, 2006.

71. Robert, J. C., and K. B. Aubrecht, “Ring-Opening Polymerization of Lactide to Form A Biodegradable Polymer”, *Journal of Chemical Education*, Vol. 85, No. 2, p. 258, 2008.

72. Wu, B., L. Tian, and Z. Wang, “Ring-Opening Polymerization of Rac-Lactide Catalyzed by Crown Ether Complexes of Sodium and Potassium Iminophenoxides”, *RSC Advances*, Vol. 7, No. 39, pp. 24055–24063, 2017.

73. Xu, J., J. Song, S. Pispas, and G. Zhang, “Metal-Free Controlled Ring-Opening Polymerization of ε-caprolactone in Bulk Using tris(pentafluorophenyl)borane as A Catalyst”, *Polymer Chemistry*, Vol. 5, No. 16, pp. 4726–4733, 2014.

APPENDIX A : COPYRIGHT NOTICES

Copyrights notices for the figures used are represented in this section.

Genes (Basel). 2020 Oct; 11(10): 1122. PMCID: PMC7598720
Published online 2020 Sep 24. doi: 10.3390/genes11101122 PMID: 32987832

Mouse Models of Human Pathogenic Variants of *TBC1D24* Associated with Non-Syndromic Deafness DFNB86 and DFNA65 and Syndromes Involving Deafness

Risa Tona,[1] Ivan A. Lopez,[2] Cristina Fenollar-Ferrer,[1,3] Rabia Faridi,[1] Claudio Anselmi,[4,5] Asma A. Khan,[6] Mohsin Shahzad,[7,8] Robert J. Morell,[9] Shoujun Gu,[10] Michael Hoa,[10] Lijin Dong,[11] Akira Ishiyama,[2] Inna A. Belyantseva,[1] Sheikh Riazuddin,[7] and Thomas B. Friedman[1,*]

▸ Author information ▸ Article notes ▾ Copyright and License information PMC Disclaimer

Figure A.1. Copyright notice for Figure 1.2.a

SPRINGER NATURE LICENSE
TERMS AND CONDITIONS

May 11, 2024

This Agreement between Bogazici University -- Goncagül Filiz ("You") and Springer Nature ("Springer Nature") consists of your license details and the terms and conditions provided by Springer Nature and Copyright Clearance Center.

License Number	5785550973892
License date	May 10, 2024
Licensed Content Publisher	Springer Nature
Licensed Content Publication	Nature Reviews Genetics
Licensed Content Title	Genetic insights into the morphogenesis of inner ear hair cells
Licensed Content Author	Gregory I. Frolenkov et al
Licensed Content Date	Jul 1, 2004
Type of Use	Thesis/Dissertation
Requestor type	academic/university or research institute
Format	electronic
Portion	figures/tables/illustrations
Number of figures/tables/illustrations	1
Would you like a high resolution image with your order?	no
Will you be translating?	no
Circulation/distribution	1 - 29
Author of this Springer Nature content	no
Title of new work	Nanoparticule Based Drug Delivery to the Inner Ear
Institution name	Boğaziçi University

Figure A.2. Copyright notice for Figure 1.2.b

J Clin Med. 2020 Jul; 9(7): 2309. PMCID: PMC7408650
Published online 2020 Jul 21. doi: 10.3390/jcm9072309 PMID: 32708116

Inner Ear Gene Therapies Take Off: Current Promises and Future Challenges

Sedigheh Delmaghani* and Aziz El-Amraoui*

▸ Author information ▸ Article notes ▾ Copyright and License information PMC Disclaimer

Figure A.3. Copyright notice for Figure 1.3

Pharmaceuticals (Basel). 2022 Sep; 15(9): 1115. PMCID: PMC9504900
Published online 2022 Sep 7. doi: 10.3390/ph15091115 PMID: 36145336

Local Delivery of Therapeutics to the Cochlea Using Nanoparticles and Other Biomaterials

Shreshtha Dash, Jian Zuo, and Peter S. Steyger*

Gary J. Stephens, Academic Editor

▸ Author information ▸ Article notes ▾ Copyright and License information PMC Disclaimer

Figure A.4. Copyright notice for Figure 1.4.

Polymeric micelles in drug delivery: An insight of the techniques for their characterization and assessment in biorelevant conditions

Author: M. Ghezzi,S. Pescina,C. Padula,P. Santi,E. Del Favero,L. Cantù,S. Nicoli

Publication: Journal of Controlled Release

Publisher: Elsevier

Date: 10 April 2021

Figure A.5. Copyright notice for Figure 1.5. and Figure 1.6

RETURN TO ISSUE | **PERSPECTIVE** | NEXT >

50th Anniversary Perspective: RAFT Polymerization—A User Guide

Sébastien Perrier*

View Author Information

Cite this: *Macromolecules* 2017, 50, 19, 7433–7447
Publication Date: September 27, 2017
https://doi.org/10.1021/acs.macromol.7b00767
Copyright © 2017 American Chemical Society. This publication is licensed under these Terms of Use.
Request reuse permissions Open Access

Article Views	Altmetric	Citations
95979	36	1025

LEARN ABOUT THESE METRICS

Figure A.6. Copyright notice for Figure 1.7